LA-UR-02-5185
Approved for public release;
distribution is unlimited.

Title: **Complex Particle and Light Fragment Emission in the Cascade-Exciton Model of Nuclear Reactions**

Author(s): Stepan G. Mashnik
Arnold J. Sierk
Konstatin K. Gudima

Submitted to: 12th Biennial RPSD Topical Meeting, April 14-18, 2002, Santa Fe, NM

http://lib-www.lanl.gov/cgi-bin/getfile?00818951.pdf

COMPLEX PARTICLE AND LIGHT FRAGMENT EMISSION IN THE CASCADE-EXCITON MODEL OF NUCLEAR REACTIONS

Stepan G. Mashnik and Arnold J. Sierk
T-16, Theoretical Division
Los Alamos National Laboratory, Los Alamos, NM 87545, USA
Tel.: 505-667-9946, E-mail: mashnik@lanl.gov
Tel.: 505-667-6784, E-mail: t2ajs@lanl.gov
Konstantin K. Gudima
Nuclear Physics Laboratory, Institute of Applied Physics,
Academy of Science of Moldova, Kishinev, MD-2028, Moldova
Tel: (373)-276-90-81, E-mail: gudima@cc.acad.md

SUMMARY

A brief description of our improvements and refinements that led from the CEM95 version of the Cascade-Exciton Model (CEM) code to CEM97 and to CEM2k is given. The increased accuracy and predictive power of the code CEM2k are shown by several examples. To describe fission and light-fragment (heavier than ^{4}He) production, the CEM2k code has been merged with the GEM2 code of Furihata. We present some results on proton-induced fragmentation and fission reactions predicted by this extended version of CEM2k. We show that merging CEM2k with GEM2 allows us to describe many fission and fragmentation reactions in addition to the spallation reactions which are already relatively well described. Nevertheless, the current version of GEM2 does not provide a completely satisfactory description of complex particle spectra, heavy-fragment emission, and spallation yields. We have initiated another approach to describe fission, complex particles and fragment emission by developing further our CEM2k code addressing specifically these problems. In this effort, we have developed our own universal approximation for inverse cross sections. We have also developed new routines to calculate Coulomb barriers and widths of emitted particles and to simulate their kinetic energy using arbitrary approximations for the inverse cross sections. To describe fission-fragment production, we have incorporated into CEM2k a thermodynamical model of fission by Stepanov. This extended version of CEM2k allows us to describe much better complex particle emission and many fission fragments, but it is still incomplete and needs further work.

I. INTRODUCTION

The design of a hybrid reactor system driven with a high-current accelerator requires information about residual nuclides that are produced by high energy protons and secondary neutrons interacting in the target and in structural materials. It is both physically and economically impossible to measure all necessary data, which is why reliable models and codes are needed. A model with a good predictive power both for the spectra of emitted particles and residual nuclide yields is the Cascade-Exciton Model (CEM) of nuclear reactions[1]. An improved version of the CEM is contained in the code CEM95[2], which is available free from the NEA/OECD, Paris. Following an increased interest in intermediate-energy nuclear data in relation to such projects as Accelerator Transmutation of nuclear Wastes (ATW), Accelerator Production of Tritium (APT), the Spallation Neutron Source (SNS), the Rare Isotope Accelerator (RIA), and others, we developed a new version of the cascade-exciton model, CEM97[3,4]. CEM97 has a number of improved physics features, uses better elementary-particle cross sections for the cascade model, and due to some significant algorithmic improvements is several times faster than CEM95. A preliminary version has been incorporated into the transport code system MCNPX, although unfortunately the MCNPX team did not include the efficiency improvements[5].

The recent GSI measurements performed using inverse kinematics for interactions of ^{208}Pb[6,7] and ^{238}U[8] at 1 GeV/nucleon and ^{197}Au at 800 MeV/nucleon[9] with liquid ^{1}H provide a very rich set of cross sections for production of practically all possible isotopes from these reactions in a "pure" form, *i.e.*, individual cross sections from a specific given bombarding isotope (or target isotope, when considering reactions in the usual kinematics, p + A). Such cross sections are much easier to compare to models than the "camouflaged" data from γ-spectrometry measurements. These are often obtained only for a natural composition of isotopes in a target and are mainly for cumulative production, where measured cross sections contain contributions nor only from the direct production of a given isotope, but also from all its decay-chain precursors. Analysis of these new data has motivated us to further improve the CEM and to develop a preliminary version of a new code, CEM2k[10,11], still under development.

In our original motivation, different versions of the CEM codes were developed to reliably describe the yields of spallation products and spectra of secondary nucleons, without a special emphasis on complex-

particle and light-fragment emission or on fission fragments in reactions with heavy targets. In fact, CEM95, CEM97, and the initial version of the CEM2k code simulate spallation only and do not calculate the process of fission, and do not provide fission fragments and a further possible evaporation of particles from them. Thus, in simulating the compound stage of a reaction, when these codes encounter a fission, they simply tabulate this event (that permits calculation of fission cross sections and fissility) and finish the calculation of this event without a subsequent treatment of fission fragments. To be able to describe nuclide production in the fission region, these codes have to be extended by incorporating a model of high energy fission (*e.g.*, in the transport code MCNPX[5], where CEM97 and CEM2k are used, they are supplemented by Atchison's fission model[12,13], often cited in the literature as the RAL model of fission).

Since many nuclear and astrophysical applications require reliable data also on complex particles (gas production) and light and/or heavy fragment production, we here address for the first time these questions with our improved cascade-exciton model and present our preliminary results on the study. We try two different ways of solving these problems and the results from both approaches are presented below after a short background on the development of the CEM.

II. FROM CEM95 TO CEM97 TO CEM2K

First, we recall the fundamental ingredients of the CEM and the main differences between the improved cascade-exciton model code CEM97[3,4] and its precursor, CEM95[2]. The CEM assumes that the reactions occur in three stages. The first stage is the IntraNuclear Cascade (INC), in which primary particles can be rescattered and produce secondary particles several times prior to absorption by, or escape from the nucleus. The excited residual nucleus remaining after the emission of the cascade particles determines the particle-hole configuration that is the starting point for the second, pre-equilibrium stage of the reaction. The subsequent relaxation of the nuclear excitation is treated in terms of the modified exciton model of pre-equilibrium decay followed by the equilibrium fission/evaporation stage of the reaction. Generally, all three components may contribute to experimentally measured particle spectra and distributions.

An important ingredient of the CEM is the criterion for transition from the intranuclear cascade to the pre-equilibrium model. In conventional cascade-evaporation models (like ISABEL and Bertini's INC used in LAHET[14], fast particles are traced down to some minimal energy, the cutoff energy T_{cut} (or one compares the duration of the cascade stage of a reaction with a cutoff time, in "time-like" INC models, such as the Liege INC[15]). This cutoff is usually about 7–10 MeV above the Fermi energy, below which particles are considered to be absorbed by the nucleus. The CEM uses a different criterion to decide when a primary particle is considered to have left the cascade.

An effective local optical absorptive potential $W_{opt.mod.}(r)$ is defined from the local interaction cross section of the particle, including Pauli-blocking effects. This imaginary potential is compared to one defined by a phenomenological global optical model $W_{opt.exp.}(r)$. We characterize the degree of similarity or difference of these imaginary potentials by the parameter

$$\mathcal{P} = \mid (W_{opt.mod.} - W_{opt.exp.})/W_{opt.exp.} \mid .$$

When $\mathcal{P}$ increases above an empirically chosen value, the particle leaves the cascade, and is then considered to be an exciton. Both CEM95 and CEM97 use the fixed value $\mathcal{P} = 0.3$. With this value, we find the cascade stage of the CEM is generally shorter than that in other cascade models.

The transition from the preequilibrium stage of a reaction to the third (evaporation) stage occurs when the probability of nuclear transitions changing the number of excitons n with $\Delta n = +2$ becomes equal to the probability of transitions in the opposite direction, with $\Delta n = -2$, *i.e.*, when the exciton model predicts an equilibration has been established in the nucleus.

The improved cascade-exciton model in the code CEM97 differs from the CEM95 version by incorporating new approximations for the elementary cross sections used in the cascade, using more precise values for nuclear masses, Q-values, binding and pairing energies, using corrected systematics for the level-density parameters, adjusting the cross sections of pion absorption on quasi-deuteron pairs inside a nucleus, allowing for nuclear transparency of pions, including the Pauli principle in the preequilibrium calculation, and implementing significant refinements and improvements in the algorithms of many subroutines, decreasing the computing time by up to a factor of 6 for heavy nuclei, which is very important when performing practical simulations with transport codes like MCNPX. On the whole, this set of improvements leads to a better description of the particle spectra and yields of residual nuclei and a better agreement with available data for a variety of nuclear reactions. Details and examples with some results from this work may be found in[3,16].

We also make a number of refinements in the calculation of the fission channel, as described in[4,17]. Besides these modifications of the CEM95 code introduced especially for a better description of fission cross sections, we have been further improving the CEM, striving for a model capable of predicting different characteristics of nuclear reactions for arbitrary targets with a wide range of incident energies. Modifications made for a better description of the preequilibrium, evaporative, and cascade stages will also affect the fission

channel. We have incorporated into the CEM the updated experimental atomic mass table by Audi and Wapstra[18], the nuclear ground-state masses (where data does not exist) and shell corrections by Möller *et al.*[19], and the pairing energy shifts from Möller, Nix, and Kratz[20] into the level-density formula. In addition, we have derived a corrected systematics for the level-density parameters using the Ignatyuk expression[21], with coefficients fitted to the data analyzed by Iljinov *et al.*[22] (we discovered that Iljinov *et al.* used $11/\sqrt{A}$ for the pairing energies Δ (see Eq. (3) in[4]) in deriving their level-density systematics instead of the value of $12/\sqrt{A}$ stated in[22]). We also derived additional semiempirical level-density-parameter systematics using the Möller *et al.*[19] ground-state microscopic corrections, both with and without the Möller, Nix, and Kratz[20] pairing gaps, and introduced into the CEM a new empirical relation to take into account the excitation-energy dependence of the ground-state shell correction in the calculation of fission barriers (see[4]).

As mentioned in the Introduction, analysis of the recent GSI measurements[6–9] has motivated us to further improve the CEM. The authors of the GSI measurements performed a comparison of their data to several codes, including LAHET[14], YIELDX[23], ISABLA (ISABEL INC code from LAHET followed by the ABLA[24] evaporation code), CASCADO[25], and the Liege INC by Cugnon[15], and encountered serious problems; none of these codes were able to accurately describe all their measurements. Most of the calculated distributions of isotopes produced as a function of neutron number were shifted toward larger masses as compared to the data. While in some disagreement with the measurements, the Liege INC and the CASCADO codes provide a better agreement with the data than LAHET, ISABLA, and YIELDX do. Being aware of this situation with the GSI data, we decided to consider them ourselves, leading to the development of CEM2k.

First, we calculated the ^{208}Pb GSI reaction[6] with the standard versions of CEM95 and CEM97 and determined[10] that though CEM95 describes quite well production of several heavy isotopes near the target (we calculate p + ^{208}Pb; therefore ^{208}Pb is a target, not a projectile as in the GSI measurements), it does not reproduce correctly the cross sections for lighter isotopes in the deep spallation region. The disagreement increases with increasing distance from the target, and all calculated curves are shifted to the heavy-mass direction, just as was obtained by the authors of the GSI measurements with the codes they tried. The results of the CEM97 code are very similar to those of CEM95 (see a figure with CEM97 results in[26]). Later on, we performed an extensive set of calculations of the same data with several more codes (HETC[27], LAHET[14] with both ISABEL and Bertini options, CASCADE[28], CASCADE/INPE[29], INUCL[30], and YIELDX[23]) and got very similar results:[26] all codes disagree with the data in the deep spallation region, the disagreement increases as one moves away from the target, and all calculated curves are shifted in the heavy-mass direction.

This means that for a given final element (Z), all models predict emission of too few neutrons. Most of the neutrons are emitted at the final (evaporation) stage of a reaction. One way to increase the number of emitted neutrons would be to increase the evaporative part of a reaction. In the CEM, this might be done in two different ways: the first would be to have a shorter preequilibrium stage, so that more excitation energy remains available for the following evaporation; the second would be to have a longer cascade stage, so that after the cascade, less exciton energy is available for the preequilibrium stage, so fewer energetic preequilibrium particles are emitted, leaving more excitation energy for the evaporative stage.

One easy way to shorten the preequilibrium stage of a reaction in CEM is to arbitrarily allow only transitions that increase the number of excitons, $\Delta n = +2$, *i.e.*, only allow the evolution of a nucleus toward the compound nucleus. In this case, the time of the equilibration will be shorter and fewer preequilibrium particles will be emitted, leaving more excitation energy for the evaporation. Such an approach is used by some other exciton models, for instance, by the Multistage Preequilibrium Model (MPM) used in LAHET[14]. Calculations using this modification to CEM97 (see Fig. 2d in[10]) provide a shift of the calculated curves in the right direction, but only very slightly improve agreement with the GSI data.

A second method of increasing evaporation is to enlarge the cascade part of a reaction; we may either enlarge the parameter $\mathcal{P}$ or remove it completely and resort to a cutoff energy T_{cut}, as is done in other INC models. Calculations have shown that a reasonable increase of $\mathcal{P}$ doesn't solve the problem. However, if we do not use $\mathcal{P}$, but instead use a cutoff energy of $T_{cut} = 1$ MeV for incident energies above the pion production threshold, the code agrees with the GSI data significantly better (see Fig. 2e in[10]). Using both these conditions leads to results that describe the p + ^{208}Pb GSI data very well. We call this approach CEM2k. An example of CEM2k results for the yield of Tm, Ir, and Tl isotopes from p + ^{208}Pb interactions compared to the GSI[6] and ITEP[31] data and with predictions by CEM95, LAHET-ISABEL, LAHET-Bertini, CASCADE, CASCADE/INPE, INUCL, and YIELDX is shown in **Fig. 1**. Similar comparisons for more isotopes may be found in[10,26,31]. We find that CEM2k agrees best with these GSI (and ITEP) data of the codes tested here and in[10,26,31].

Finding a good agreement of CEM2k with the isotope production, we wish to see how well it describes spectra of secondary particles in comparison

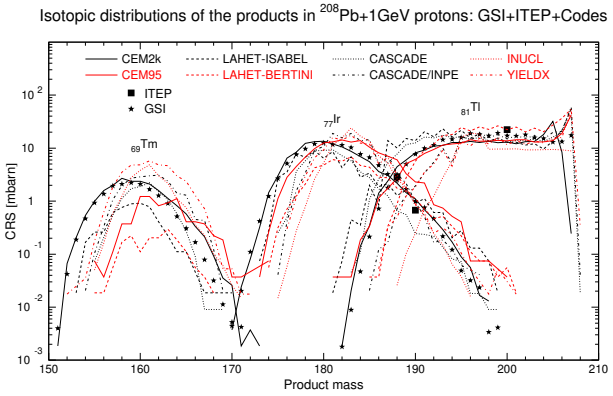

Figure 1. Mass distributions for independent production of Tm, Ir, and Tl isotopes from 1 GeV protons colliding with ^{208}Pb. Stars are GSI measurements[6], while squares show ITEP data[31]. The calculations are identified as: CEM2k—our results, CEM95[2], LAHET-ISABEL[14], LAHET-Bertini[14], CASCADE/INPE[29], CASCADE[28], INUCL[30], and YIELDX[23].

with CEM97. **Figure 2** shows examples of neutron spectra from interactions of protons with the same target, ^{208}Pb at 0.8 and 1.5 GeV (we do not know of measurements of spectra at 1 GeV, the energy of the isotope-production data). We see that CEM2k describes spectra of secondary neutrons comparably to CEM97, even possibly a little better at larger angles.

So this preliminary version of CEM2k describes both the GSI data from ^{208}Pb interactions with p at 1 GeV/nucleon and the spectra of emitted neutrons from p+^{208}Pb at 0.8 and 1.5 GeV better than its precursor CEM97.

We use CEM2k as fixed from our analysis of the ^{208}Pb data[6,7] without further modifications to calculate the ^{197}Au[9] and ^{238}U[8] GSI measurements. An example of the yield of several isotopes from ^{197}Au calculated by CEM2k is shown in **Fig. 3** together with standard CEM97 predictions and calculations by the LAHET-Bertini and YIELDX codes from[9]. We see that just as in the case of the ^{208}Pb data, CEM2k agrees best with the ^{197}Au data in the spallation region compared to the other codes tested here. Several more results for ^{197}Au and ^{238}U and their detailed discussion may be found in[10].

Besides the changes to CEM97 mentioned above, we also made a number of other improvements and refinements, such as imposing momentum-energy conservation for each simulated event (the Monte Carlo algorithm previously used in CEM provides momentum-energy conservation only statistically, on the average, but not exactly for the cascade stage of each event); using real binding energies for nucleons at the cascade stage instead of the approximation of a constant separation energy of 7 MeV used in previous versions of

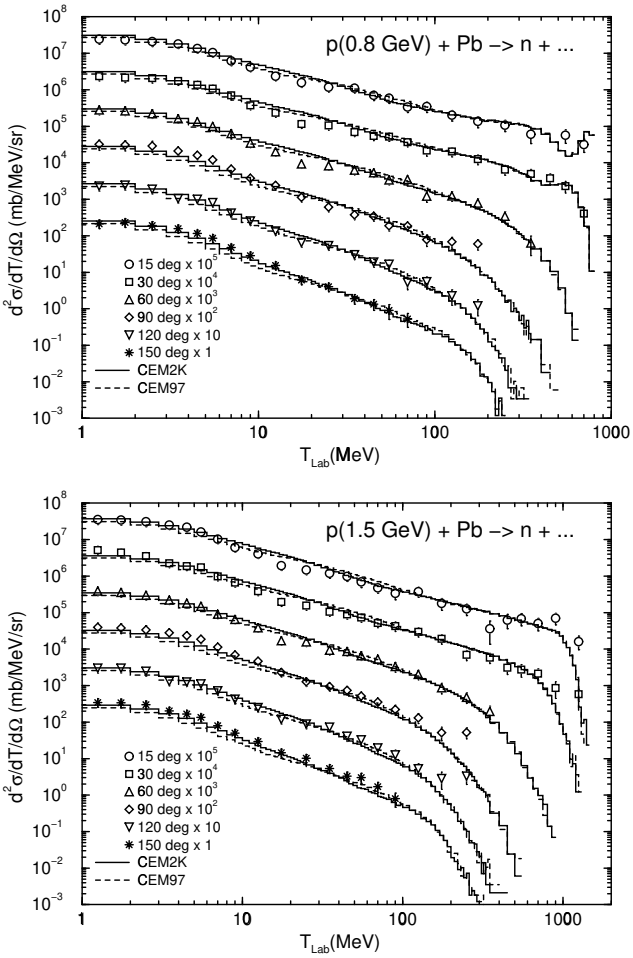

Figure 2. Comparison of measured[32] double differential cross sections of neutrons from 0.8 and 1.5 GeV protons on Pb to CEM2k and CEM97 calculations.

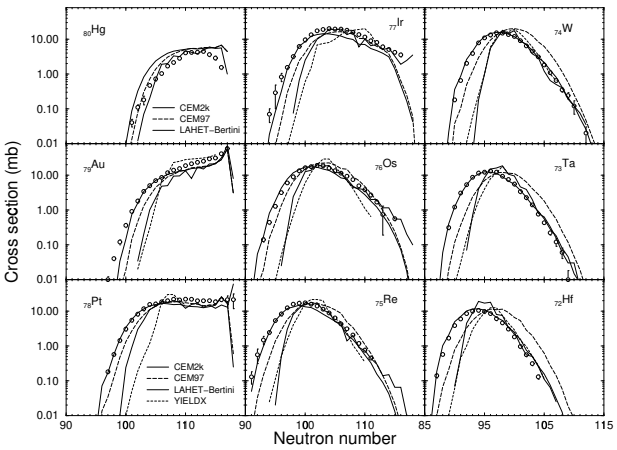

Figure 3. Isotopic distributions of spallation products from the reaction ^{197}Au + p at 800 A MeV from mercury to hafnium. Open circles are the GSI data[9], CEM2k (thick solid curves) and CEM97 (thick dashed curves) are our present calculations, LAHET-Bertini (thin solid curves) and YIELDX (thin dashed curves) are calculations from[9].

the CEM; and using reduced masses of particles in the calculation of their emission widths instead of using the approximation of no recoil used previously. In Ref[11]. we have shown that these refinements (which involve no further parameter fitting), while only improving slightly the agreement with the GSI measurements (and other data on medium and heavy targets), are crucial for light targets, especially when calculating ^{4}He and other fragment emission from light nuclei. This is especially important for applications where gas production is calculated.

Another improvement important for applications is better representing the total reaction cross section. Previous versions of CEM (just like many other INC-type models) calculate the total reaction cross section, σ_{in} using the geometrical cross section, σ_{geom}, and the number of inelastic, N_{in}, and elastic, N_{el}, simulated events, namely: $\sigma_{in} = \sigma_{geom} N_{in}/(N_{in} + N_{el})$. This approach provides a good agreement with available data at incident energies above about 100 MeV, but is not reliable at lower bombarding energies. To address this problem, we have incorporated into CEM2k the NASA systematics by Tripathi *et al.*[33] for all incident protons and neutrons with energies above the maximum in the NASA reaction cross sections, and the Kalbach systematics[34] for neutrons of lower energy. As shown in **Fig. 4**, we can describe much better with CEM2k the total reaction cross sections (and correspondingly any other partial cross sections) for n- and p-induced reactions, especially at energies below about 100 MeV.

III. MERGING CEM2K WITH GEM2

As a first attempt to describe with CEM2k both emission of intermediate-mass fragments heavier than ^{4}He and production of heavy fragments from fission, we merged CEM2k with the Generalized Evaporation Model (GEM) code by Furihata[37,38]. GEM is an extension by Furihata of the Dostrovsky evaporation model[39] as implemented in LAHET[14] to include up to 66 types of particles and fragments that can be evaporated from an excited compound nucleus plus a modification of the version of Atchison's fission model[12,13] used in LAHET. Many of the parameters were adjusted for a better description of fission reactions when using it in conjunction with the extended evaporation model. We merged GEM2 (the last update of the GEM code) with CEM2k as follows: we calculate the cascade and preequilibrium stages of a reaction with our CEM2k, then we describe the subsequent evaporation of particles and fragments and fission from the remaining excited compound nuclei using GEM2. To understand the role of preequilibrium particle emission, we performed calculations of all the reactions we tested both with emission of preequilibrium particles and without them, *i.e.*, going directly to GEM2 after the intranuclear cascade stage of a reaction described by CEM2k.

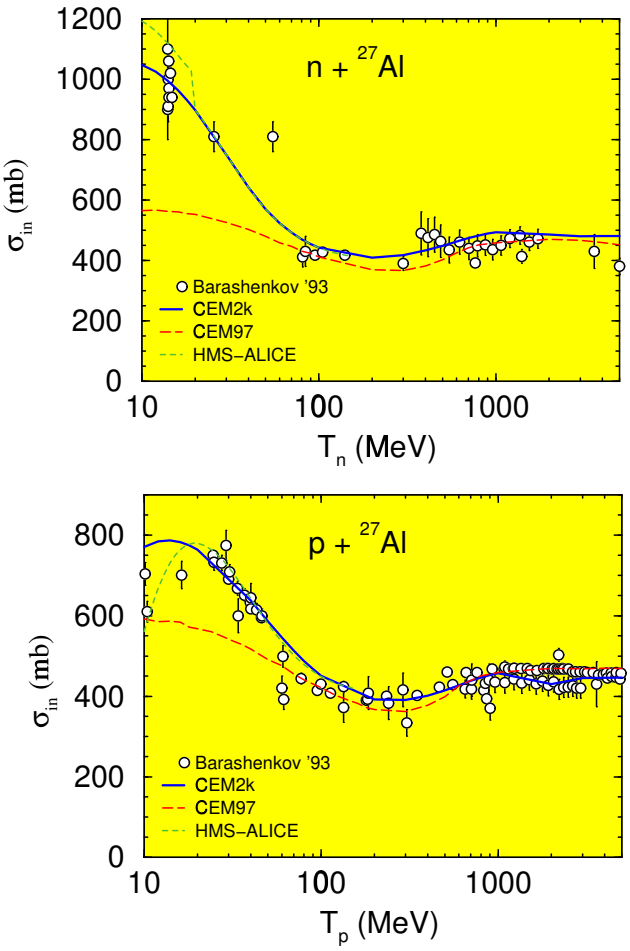

Figure 4. Total reaction cross sections for n- and p-induced reactions on Al calculated by CEM2k and CEM97 compared with experimental data compiled by Barashenkov[35] and calculations from the HMS-ALICE code[36].

A very detailed description of the GEM, together with a large amount of results obtained for many reactions using GEM coupled either with the Bertini or ISABEL INC models in LAHET may be found in[37,38]. Therefore, we present here only the main features of GEM, following mainly[38] and using as well useful information obtained in private communications from Dr. Furihata.

A. Evaporation Model in GEM

Furihata did not change in GEM the general algorithms used in LAHET to simulate evaporation and fission. The decay widths of evaporated particles and fragments are estimated using the classical Weisskopf-Ewing statistical model[40]. In this approach, the decay probability P_j for the emission of a particle j from a parent compound nucleus i with the total kinetic energy in the center-of-mass system between ϵ and $\epsilon + d\epsilon$ is

$$P_j(\epsilon)d\epsilon = g_j \sigma_{inv}(\epsilon) \frac{\rho_d(E - Q - \epsilon)}{\rho_i(E)} \epsilon d\epsilon, \qquad (1)$$

where E [MeV] is the excitation energy of the parent nucleus i with mass A_i and charge Z_i, and d denotes a daughter nucleus with mass A_d and charge Z_d produced after the emission of ejectile j with mass A_j and charge Z_j in its ground state. σ_{inv} is the cross section for the inverse reaction, ρ_i and ρ_d are the level densities [MeV]$^{-1}$ of the parent and the daughter nucleus, respectively. $g_j = (2S_j + 1)m_j/\pi^2\hbar^2$, where S_j is the spin and m_j is the mass of the emitted particle j. The Q-value is calculated using the excess mass $M(A, Z)$ as $Q = M(A_j, Z_j) + M(A_d, Z_d) - M(A_i, Z_i)$. In GEM, four mass tables are used to calculate Q-values, according to the following priority: (1) the Audi-Wapstra mass table[18], (2) theoretical masses calculated by Möller *et al.*[19], (3) theoretical masses calculated by Comay *et al.*[41], (4) the mass excess calculated using the old Cameron formula[42]. As does LAHET, GEM uses Dostrovsky's formula[39] to calculate the inverse cross section σ_{inv} for all emitted particles and fragments

$$\sigma_{inv}(\epsilon) = \sigma_g \alpha \left(1 + \frac{\beta}{\epsilon}\right) \ , \qquad (2)$$

which is often written as

$$\sigma_{inv}(\epsilon) = \begin{cases} \sigma_g c_n (1 + b/\epsilon) & \text{for neutrons} \\ \sigma_g c_j (1 - V/\epsilon) & \text{for charged particles} \ , \end{cases}$$

where $\sigma_g = \pi R_b^2$ [fm^2] is the geometrical cross section, and

$$V = k_j Z_j Z_d e^2 / R_c \qquad (3)$$

is the Coulomb barrier in MeV.

The new ingredient in GEM in comparison with LAHET which considers evaporation of only 6 particles (n, p, d, t, ^{3}He, and ^{4}He) is that Furihata included the possibility of evaporation of up to 66 types of particles and fragments and incorporated into GEM several sets of parameters b, c_j, k_j, R_b, and R_c for each particle.

The 66 ejectiles considered by GEM for evaporation are selected to satisfy the following criteria: (1) isotopes with $Z_j \leq 12$; (2) naturally existing isotopes or isotopes near the stability line; (3) isotopes with half-lives longer than 1 ms. All the 66 ejectiles considered by GEM are shown in Table 1.

Table 1. The ejectiles considered by GEM

Z_j	Ejectiles						
0	n						
1	p	d	t				
2	^{3}He	^{4}He	^{6}He	^{8}He			
3	^{6}Li	^{7}Li	^{8}Li	^{9}Li			
4	^{7}Be	^{9}Be	^{10}Be	^{11}Be	^{12}Be		
5	^{8}B	^{10}B	^{11}B	^{12}B	^{13}B		
6	^{10}C	^{11}C	^{12}C	^{13}C	^{14}C	^{15}C	^{16}C
7	^{12}N	^{13}N	^{14}N	^{15}N	^{16}N	^{17}N	
8	^{14}O	^{15}O	^{16}O	^{17}O	^{18}O	^{19}O	^{20}O
9	^{17}F	^{18}F	^{19}F	^{20}F	^{21}F		
10	^{18}Ne	^{19}Ne	^{20}Ne	^{21}Ne	^{22}Ne	^{23}Ne	^{24}Ne
11	^{21}Na	^{22}Na	^{23}Na	^{24}Na	^{25}Na		
12	^{22}Mg	^{23}Mg	^{24}Mg	^{25}Mg	^{26}Mg	^{27}Mg	^{28}Mg

GEM includes several options for the parameter set in expressions (2,3):

1) The "simple" parameter set is given as $c_n = c_j = k_j = 1$ $b = 0$, and $R_b = R_c = r_0(A_j^{1/3} + A_d^{1/3})$ [fm]; users need to input r_0.

2) The "precise" parameter set is used in GEM as default, and we use this set in our present work.

A) For all light ejectiles up to α ($A_j \leq 4$), the parameters determined by Dostrovsky *et al.*[39] are used in GEM, namely: $c_n = 0.76 + c_a A_d^{-1/3}$, $b = (b_a A_d^{-2/3} - 0.050)/(0.76 + c_a A_d^{-1/3})$ (and $b = 0$ for $A_d \geq 192$), where $c_a = 1.93$ and $b_a = 1.66$, $c_p = 1 + c$, $c_d = 1 + c/2$, $c_t = 1 + c/3$, $c_{^3He} = c_\alpha = 0$, $k_p = k$, $k_d = k + 0.06$, $k_t = k + 0.12$, $k_{^3He} = k_\alpha - 0.06$, where c, k, and k_α are listed in Table 2 for a set of Z_d. Between the Z_d values listed in Table 2, c, k, and k_α are interpolated linearly.The nuclear distances are given by $R_b = 1.5A^{1/3}$ for neutrons and protons, and $1.5(A_d^{1/3} + A_j^{1/3})$ for d, t, ^{3}He, and α.

Table 2. k, k_α, and c parameters used in GEM

Z_d	k	k_α	c
≤ 20	0.51	0.81	0.0
30	0.60	0.85	-0.06
40	0.66	0.89	-0.10
≥ 50	0.68	0.93	-0.10

The nuclear distance for the Coulomb barrier is expressed as $R_c = R_d + R_j$, where $R_d = r_0^c A^{1/3}$, $r_0^c = 1.7$, and $R_j = 0$ for neutrons and protons, and $R_j = 1.2$ for d, t, ^{3}He, and ^{4}He. We note that several of these parameters are similar to the original values published by Dostrovsky *et al.*[39] (and used, for example in our CEM codes) but not exactly the same. Dostrovsky *et al.*[39] had $c_a = 2.2$, $b_a = 2.12$, and $r_0^c = 1.5$. Also, for the k, k_α, and c parameters shown in Table 2, they had slightly different values, shown in Table 3.

Table 3. k_p, c_p, k_α, and c_α parameters from Ref.[39]

Z_d	k_p	c_p	k_α	c_α
10	0.42	0.50	0.68	0.10
20	0.58	0.28	0.82	0.10
30	0.68	0.20	0.91	0.10
50	0.77	0.15	0.97	0.08
≥ 70	0.80	0.10	0.98	0.06

B) For fragments heavier that α ($A_j \geq 4$), "the precise" parameters of GEM use values by Matsuse *et al.*[43], namely: $c_j = k = 1$, $R_b = R_0(A_j) + R_0(A_d) + 2.85$ [fm], $R_c = R_0(A_j) + R_0(A_d) + 3.75$ [fm], where $R_0(A) = 1.12A^{1/3} - 0.86A^{-1/3}$.

3) The upgraded version of GEM realized in the code GEM2 contains two other options for the parameters of the inverse cross sections.

A) A set of parameters due to Furihata for light ejectiles in combination with Matsuse's parameters for fragments heavier than α. Furihata and Nakamura determined k_j for p, d, t, ^{3}He, and α as follows:[44]

$$k_j = c_1 \log(Z_d) + c_2 \log(A_d) + c_3.$$

The coefficients c_1, c_2, and c_3 for each ejectile are shown in Table 4.

Table 4. c_1, c_2, and c_3 for p, d, t, ^{3}He, and α from[44]

Ejectile	c_1	c_2	c_3
p	0.0615	0.0167	0.3227
d	0.0556	0.0135	0.4067
t	0.0530	0.0134	0.4374
^{3}He	0.0484	0.0122	0.4938
α	0.0468	0.0122	0.5120

When these parameters are chosen in GEM2, the following nuclear radius R is used in the calculation of V and σ_g:

$$R = \begin{cases} 0 & \text{for } A = 1\ , \\ 1.2 & \text{for } 2 \leq A \leq 4\ , \\ 2.02 & \text{for } 5 \leq A \leq 6\ , \\ 2.42 & \text{for } A = 7\ , \\ 2.83 & \text{for } A = 8\ , \\ 3.25 & \text{for } A = 9\ , \\ 1.414A_d^{1/3} + 1 & \text{for } A \geq 10\ . \end{cases}$$

B) The second new option in GEM2 is to use Furihata's parameters for light ejectiles up to α and the Botvina *et al.*[45] parameterization for inverse cross sections for heavier ejectiles. Botvina *et al.*[45] found that σ_{inv} can be expressed as

$$\sigma_{inv} = \sigma_g \begin{cases} (1 - V/\epsilon) & \text{for } \epsilon \geq V + 1 \text{ [MeV]}, \\ \frac{e^{\alpha(\epsilon - V - 1)}}{V+1} & \text{for } \epsilon < V + 1 \text{ [MeV]}, \end{cases} \quad (4)$$

where

$$\alpha = 0.869 + 9.91/Z_j,$$

$$V = \frac{Z_j Z_d}{r_0^b (A_j^{1/3} + A_d^{1/3})},$$

$$r_0^b = 2.173 \frac{1 + 6.103 \times 10^{-3} Z_j Z_d}{1 + 9.443 \times 10^{-3} Z_j Z_d} \text{ [fm]}.$$

The expression of σ_{inv} for $\epsilon < V + 1$ shows the fusion reaction in the sub-barrier region. When using Eq. (4) instead of Eq. (2), the total decay width for a fragment emission can not be calculated analytically. Therefore, the total decay width must be calculated numerically and takes much CPU time.

The total decay width Γ_j is calculated by integrating Eq. (1) with respect to the total kinetic energy ϵ from the Coulomb barrier V up to the maximum possible value, $(E - Q)$. The good feature of Dostrovsky's approximation for the inverse cross sections, Eq. (2), is its simple energy dependence that allows the analytic integration of Eq. (1). By using Eq. (2) for σ_{inv}, the total decay width for the particle emission is

$$\Gamma_j = \frac{g_j \sigma_g \alpha}{\rho_i(E)} \int_V^{E-Q} \epsilon \left(1 + \frac{\beta}{\epsilon}\right) \rho_d(E - Q - \epsilon) d\epsilon. \quad (5)$$

The level density $\rho(E)$ is calculated in GEM according to the Fermi-gas model using the expression[46]

$$\rho(E) = \frac{\pi}{12} \frac{\exp(2\sqrt{a(E - \delta)})}{a^{1/4}(E - \delta)^{5/4}}, \quad (6)$$

where a is the level density parameter and δ is the pairing energy in MeV. As does LAHET, GEM uses the δ values evaluated by Cook *et al.*[47] For those values not evaluated by Cook *et al.*, δ's from Gilbert and Cameron[46] are used instead. The simplest option for the level density parameter in GEM is $a = A_d/8$ [MeV^{-1}], but the default is the Gilbert-Cameron-Cook-Ignatyuk (GCCI) parameterization from LAHET:[14]

$$a = \tilde{a} \frac{1 - e^{-u}}{u} + a_I \left(1 - \frac{1 - e^{-u}}{u}\right), \quad (7)$$

where $u = 0.05(E - \delta)$, and

$$a_I = (0.1375 - 8.36 \times 10^{-5} A_d) \times A_d,$$

$$\tilde{a} = \begin{cases} A_d/8 & \text{for } Z_d < 9 \text{ or } N_d < 9, \\ A_d(a' + 0.00917S) & \text{for others.} \end{cases}$$

For deformed nuclei with $54 \leq Z_d \leq 78$, $86 \leq Z_d \leq 98$, $86 \leq N_d \leq 122$, or $130 \leq N_d \leq 150$, $a' = 0.12$ while $a' = 0.142$ for other nuclei. The shell corrections S is expressed as a sum of separate contributions from neutrons and protons, *i.e.* $S = S(Z_d) + S(N_d)$ from[46,47] and are tabulated in[38].

The level density is calculated using Eq. (6) only for high excitation energies, $E \geq E_x$, where $E_x = U_x + \delta$ and $U_x = 2.5 + 150/A_d$ (all energies are in MeV). At lower excitation energies, the following[46] is used for the level density:

$$\rho(E) = \frac{\pi}{12} \frac{1}{T} \exp((E - E_0)/T), \tag{8}$$

where T in the nuclear temperature defined as $1/T = \sqrt{a/U_x} - 1.5/U_x$. To provide a smooth connection of Eqs. (6) and (8) at $E = E_x$, E_0 is defined as $E_0 = E_x - T(\log T - 0.25 \log a - 1.25 \log U_x + 2\sqrt{aU_x})$.

For $E - Q - V < E_x$, substituting Eq. (8) into Eq. (5) we can calculate the integral analytically, if we neglect the dependence of the level density parameter a on E:

$$\Gamma_j = \frac{\pi g_j \sigma_g \alpha}{12 \rho_i(E)} \{I_1(t,t) + (\beta + V) I_0(t)\}, \tag{9}$$

where $I_0(t)$ and $I_1(t, t_x)$ are expressed as

$$I_0(t) = e^{-E_0/T}(e^t - 1),$$
$$I_1(t, t_x) = e^{-E_0/T} T\{(t - t_x + 1)e^{t_x} - t - 1\},$$

where $t = (E - Q - V)/T$ and $t_x = E_x/T$. For $E - Q - V \geq E_x$, the integral of Eq. (5) cannot be solved analytically because of the denominator in Eq. (6). However, it is approximated as

$$\Gamma_j = \frac{\pi g_j \sigma_g \alpha}{12 \rho_i(E)} [I_1(t, t_x) + I_3(s, s_x) e^s + (\beta + V) \times \{I_0(t_x) - I_2(s, s_x) e^s\}], \tag{10}$$

where $I_2(s, s_x)$ and $I_3(s, s_x)$ are given by

$$I_2(s, s_x) = 2\sqrt{2}\{s^{-3/2} + 1.5 s^{-5/2} + 3.75 s^{-7/2} - (s_x^{-3/2} + 1.5 s_x^{-5/2} + 3.75 s_x^{-7/2}) e^{s_x - s}\},$$

$$\begin{aligned} I_3(s, s_x) = (\sqrt{2}a)^{-1} [&2s^{-1/2} + 4s^{-3/2} + 13.5 s^{-5/2} \\ &+ 60.0 s^{-7/2} + 325.125 s^{-9/2} \\ &- \{(s^2 - s_x^2) s_x^{-3/2} + (1.5 s^2 + 0.5 s_x^2) s_x^{-5/2} \\ &+ (3.75 s^2 + 0.25 s_x^2) s_x^{-7/2} \\ &+ (12.875 s^2 + 0.625 s_x^2) s_x^{-9/2} \\ &+ (59.0625 s^2 + 0.9375 s_x^2) s_x^{-11/2} \\ &+ (324.8 s_x^2 + 3.28 s_x^2) s_x^{-13/2}\} e^{s_x - s}], \end{aligned}$$

with $s = 2\sqrt{a(E - Q - V - \delta)}$ and $s_x = 2\sqrt{a(E_x - \delta)}$.

The ejectile j to be evaporated is selected in GEM by the Monte Carlo method according to the probability distribution calculated as $P_j = \Gamma_j / \sum_j \Gamma_j$, where Γ_j is given by Eqs. (9) or (10). The total kinetic energy ϵ of the emitted particle j and the recoil energy of the daughter nucleus is chosen according to the probability distribution given by Eq. (1). The angular distribution of ejectiles is simulated to be isotropic in the center-of-mass system.

According to Friedman and Lynch[48], it is important to include excited states in the particle emitted via the evaporation process along with evaporation of particles in their ground states, because it greatly enhances the yield of heavy particles. Taking this into consideration, GEM includes evaporation of complex particles and light fragments both in the ground states and excited states. An excited state of a fragment is included in calculations if its half-lifetime $T_{1/2}(s)$ satisfies the following condition:

$$\frac{T_{1/2}}{\ln 2} > \frac{\hbar}{\Gamma_j^*}, \tag{11}$$

where Γ_j^* is the decay width of the excited particle (resonance). GEM calculates Γ_j^* in the same manner as for a ground-state particle emission. The Q-value for the resonance emission is expressed as $Q^* = Q + E_j^*$, where E_J^* is the excitation energy of the resonance. The spin state of the resonance S_j^* is used in the calculation of g_j, instead of the spin of the ground state S_j. GEM uses the ground state masses m_j for excited states because the difference between the masses is negligible.

Instead of treating a resonance as an independent particle, GEM simply enhances the decay width Γ_j of the ground state particle emission as follows:

$$\Gamma_j = \Gamma_j^0 + \sum_n \Gamma_j^n, \tag{12}$$

where Γ_j^0 is the decay width of the ground state particle emission, and Γ_j^n is that of the nth excited state of the particle j emission which satisfies Eq. (11).

The total kinetic energy distribution of the excited particles is assumed to be the same as that of the ground state particle emission. S_j^*, E_j^*, and $T_{1/2}$ used in GEM are extracted from the Evaluated Nuclear Structure Data File (ENSDF) database maintained by the National Nuclear Data Center at Brookhaven National Laboratory[49].

Note that when including evaporation of up to 66 particles in GEM, its running time increases many times compared to the case when evaporating only 6 particles, up to ^{4}He. The major particles emitted from an excited nucleus are n, p, d, t, ^{3}He, and ^{4}He. For most

of the cases, the total emission probability of particles heavier than α is negligible compared to those for the emission of light ejectiles. To keep the GEM running time to a reasonable level, calculations of probability of emission of particles heavier than α are done only for 5% of simulated evaporations for $A_i > 40$, 7% of simulated evaporations for $30 < A_i \leq 40$, and 30% of simulated evaporations for $20 < A_i \leq 30$. This empirical criterion was determined by Furihata from actual simulations[38].

B. Fission Model in GEM

The fission model used in GEM is based on Atchison's model[12,13] as implemented in LAHET[14], often referred in the literature as the Rutherford Appleton Laboratory (RAL) model, which is where Atchison developed it. There are two choices of parameters for the fission model: one of them is the original parameter set by Atchison[12,13] as implemented in LAHET[14], and the other is a parameter set evaluated by Furihata[37,38].

B.1. Fission Probability. The Atchison fission model is designed to only describe fission of nuclei with $Z \geq 70$. It assumes that fission competes only with neutron emission, *i.e.*, from the widths Γ_j of n, p, d, t, ^{3}He, and ^{4}He, the RAL code calculates the probability of evaporation of any particle. When a charged particle is selected to be evaporated, no fission competition is taken into account. When a neutron is selected to be evaporated, the code does not actually simulate its evaporation, instead it considers that fission may compete, and chooses either fission or evaporation of a neutron according to the fission probability P_f. This quantity is treated by the RAL code differently for the elements above and below $Z = 89$. The reasons Atchison split the calculation of the fission probability P_f are: (1) there is very little experimental information on fission in the region $Z = 85$ to 88, (2) the marked rise in the fission barrier for nuclei with Z^2/A below about 34 (see Fig. 2 in[13]) together with the disappearance of asymmetric mass splitting, indicates that a change in the character of the fission process occurs. If experimental information were available, a split between regions about $Z^2/A \approx 34$ would more sensible[13].

1) $70 \leq Z_j \leq 88$. For fissioning nuclei with $70 \leq Z_j \leq 88$, GEM uses the original Atchison calculation of the neutron emission width Γ_n and fission width Γ_f to estimate the fission probability as

$$P_f = \frac{\Gamma_f}{\Gamma_f + \Gamma_n} = \frac{1}{1 + \Gamma_n/\Gamma_f}. \quad (13)$$

Atchison uses[12,13] the Weisskopf and Ewing statistical model[40] with an energy-independent preexponential factor for the level density (see Eq. (6)) and Dostrovsky's[39] inverse cross section for neutrons and estimates the neutron width Γ_n as

$$\Gamma_n = 0.352\big(1.68J_0 + 1.93A_i^{1/3}J_1 + A_i^{2/3}(0.76J_1 - 0.05J_0)\big), \quad (14)$$

where J_0 and J_1 are functions of the level density parameter a_n and $s_n(= 2\sqrt{a_n(E - Q_n - \delta)})$ as

$$J_0 = \frac{(s_n - 1)e^{s_n} + 1}{2a_n},$$

$$J_1 = \frac{(2s_n^2 - 6s_n + 6)e^{s_n} + s_n^2 - 6}{8a_n^2}.$$

Note that the RAL model uses a fixed value for the level density parameter a_n, namely

$$a_n = (A_i - 1)/8, \quad (15)$$

and this approximation is kept in GEM when calculating the fission probability according to Eq. (13), though it differs from the GCCI parameterization (7) used in GEM to calculate particle evaporation widths. The fission width for nuclei with $70 \leq Z_j \leq 88$ is calculated in the RAL model and in GEM as

$$\Gamma_f = \frac{(s_f - 1)e^{s_f} + 1}{a_f}, \quad (16)$$

where $s_f = 2\sqrt{a_f(E - B_f - \delta)}$ and the level density parameter in the fission mode a_f is fitted by Atchison to describe the measured Γ_f/Γ_n as:[13]

$$a_f = a_n\Big(1.08926 + 0.01098(\chi - 31.08551)^2\Big), \quad (17)$$

and $\chi = Z^2/A$. The fission barriers B_f [MeV] are estimated as

$$B_f = Q_n + 321.2 - 16.7\frac{Z_i^2}{A} + 0.218\left(\frac{Z_i^2}{A_i}\right)^2. \quad (18)$$

Note that neither the angular momentum nor the excitation energy of the nucleus are taken into account in the estimate of the fission barriers.

2) $Z_j \geq 89$. For heavy fissioning nuclei with $Z_j \geq 89$ GEM follows the RAL model[12,13] and does not calculate at all the fission width Γ_f and does not use Eq. (13) to estimate the fission probability P_f. Instead, the following semi-empirical expression obtained by Atchison[12,13] by approximating the experimental values of Γ_n/Γ_f published by Vandenbosch and Huizenga[50] is used to calculate the fission probability:

$$\log(\Gamma_n/\Gamma_f) = C(Z_i)(A_i - A_0(Z_i)), \quad (19)$$

where $C(Z)$ and $A_0(Z)$ are constants dependent on the nuclear charge Z only. The values of these constants are those used in the current version of LAHET[14] and are tabulated in Table 5 (note that some adjustments of these values have been done since Atchison's papers[12,13] were published).

Table 5. $C(Z)$ and $A_0(Z)$ values used in GEM

Z	$C(Z)$	$A_0(Z)$
89	0.23000	219.40
90	0.23300	226.90
91	0.12225	229.75
92	0.14727	234.04
93	0.13559	238.88
94	0.15735	241.34
95	0.16597	243.04
96	0.17589	245.52
97	0.18018	246.84
98	0.19568	250.18
99	0.16313	254.00
100	0.17123	257.80
101	0.17123	261.30
102	0.17123	264.80
103	0.17123	268.30
104	0.17123	271.80
105	0.17123	275.30
106	0.17123	278.80

In this approach the fission probability P_f is independent of the excitation energy of the fissioning nucleus and its angular momentum.

B.2. Mass Distribution. The selection of the mass of the fission fragments depends on whether the fission is symmetric or asymmetric. For a pre-fission nucleus with $Z_i^2/A_i \leq 35$, only symmetric fission is allowed. For $Z_i^2/A_i > 35$, both symmetric and asymmetric fission are allowed, depending on the excitation energy of the fissioning nucleus. No new parameters were determined for asymmetric fission in GEM.

For nuclei with $Z_i^2/A_i > 35$, whether the fission is symmetric or not is determined by the asymmetric fission probability P_{asy}

$$P_{asy} = \frac{4870e^{-0.36E}}{1+4870e^{-0.36E}}. \tag{20}$$

B.2.a. Asymmetric fission. For asymmetric fission, the mass of one of the post-fission fragments A_1 is selected from a Gaussian distribution of mean $A_f = 140$ and width $\sigma_M = 6.5$. The mass of the second fragment is $A_2 = A_i - A_1$.

B.2.b. Symmetric fission. For symmetric fission, A_1 is selected from the Gaussian distribution of mean $A_f = A_i/2$ and two options for the width σ_M as described below.

The first option for choosing σ_M is the original Atchison approximation:

$$\sigma_M = \begin{cases} 3.97 + 0.425(E-B_f) - 0.00212(E-B_f)^2, \\ 25.27, \end{cases} \tag{21}$$

for $(E - B_f)$ below or above 100 MeV, respectively. In this expression all values are in MeV and the fission barriers B_f are calculated according to Eq. (18) for nuclei with $Z_i \leq 88$. For nuclei with $Z_i > 88$, the expression by Neuzil and Fairhall[51] is used:

$$B_f = C - 0.36(Z_i^2/A_i), \tag{22}$$

where $C = 18.8, 18.1, 18.1$, and 18.5 [MeV] for odd-odd, even-odd, odd-even, and even-even nuclei, respectively.

The second option in GEM for σ_M (used here) was found by Furihata[37,38] as:

$$\sigma_M = C_3(Z_i^2/A_i)^2 + C_4(Z_i^2/A_i) + C_5(E-B_f) + C_6. \tag{23}$$

The constants $C_3 = 0.122$, $C_4 = -7.77$, $C_5 = 3.32 \times 10^{-2}$, and $C_6 = 134.0$ were obtained by fitting with GEM the recent Russian collection of experimental fission-fragment mass distributions[52]. In this expression, the fission barriers B_f by Myers and Swiatecki[53] are used. More details may be found in Ref.[38]

B.3. Charge Distribution. The charge distribution of fission fragments is assumed to be a Gaussian distribution of mean Z_f and width σ_Z. Z_f is expressed as

$$Z_f = \frac{Z_i + Z_1' - Z_2'}{2}, \tag{24}$$

where

$$Z_l' = \frac{65.5A_l}{131 + A_l^{2/3}}, l = 1 \text{ or } 2. \tag{25}$$

The original Atchison model uses $\sigma_Z = 2.0$. An investigation by Furihata[38] suggests that $\sigma_Z = 0.75$ provides a better agreement with data; therefore $\sigma_Z = 0.75$ is used in GEM and in our calculations.

B.4. Kinetic Energy Distribution. The kinetic energy of fission fragments [MeV] is determined by a Gaussian distribution with mean ϵ_f and width σ_{ϵ_f}.

The original parameters in the Atchison model are:

$$\epsilon_f = 0.133Z_i^2/A_i^{1/3} - 11.4,$$

$$\sigma_{\epsilon_f} = 0.084\epsilon_f.$$

Furihata's parameters in GEM, which we also use, are:

$$\epsilon_f = \begin{cases} 0.131 Z_i^2/A_i^{1/3}, \\ 0.104 Z_i^2/A_i^{1/3} + 24.3, \end{cases} \quad (26)$$

for $Z_i^2/A_i^{1/3} \leq 900$ and $900 < Z_i^2/A_i^{1/3} \leq 1800$, respectively, according to Rusanov et al.[52] By fitting the experimental data by Itkis et al.[54], Furihata found the following expression for σ_{ϵ_f}

$$\sigma_{\epsilon_f} = \begin{cases} C_1(Z_i^2/A_i^{1/3} - 1000) + C_2, \\ C_2, \end{cases} \quad (27)$$

for $Z_i^2/A_i^{1/3}$ above and below 1000, respectively, and the values of the fitted constants are $C_1 = 5.70 \times 10^{-4}$ and $C_2 = 86.5$ The experimental data used by Furihata for fitting are the extrapolated values to the nuclear temperature 1.5 MeV by Itkis *et al.*[54] More details may be found in[38].

We note that Atchison also has modified his original version using recent data and published[55] an improved (and more complicated) parameterization for many quantities and distributions in his model, but these modifications[55] are not yet included either in LAHET or in GEM.

C. Results from CEM2k+GEM2

We have merged the GEM2 code with our CEM2k, initially keeping all the default options in GEM2. We began by concentrating on an analysis of the recent GSI measurements in inverse kinematics[6–9] as the richest and best data set for testing this kind of model. As mentioned above, to understand the role of preequilibrium particle emission, we performed calculations of all the reactions we tested both taking into account preequilibrium particle emission and ignoring it, *i.e.*, going directly to GEM2 after the intranuclear cascade stage of a reaction described by CEM2k. The size of the present paper allows us to present only a few results for one reaction measured at GSI, which we choose to be p(800 MeV) + Au[9]. Results for other reactions may be found in[56].

If we merge GEM2 with CEM2k without any modifications, the new code does not describe correctly the fission cross section (and the yields of fission fragments) whether we take into account preequilibrium emission (see the dashed red line on Fig. 5) or not (see the dashed blue line on Fig. 5). Such results were anticipated, as Atchison fitted the parameters of his RAL fission model when it was coupled with the Bertini INC[57] which differs from our INC. In addition, he did not model preequilibrium emission. Therefore, the distributions of fissioning nuclei in A, Z, and excitation energy E^* simulated by Atchison differ significantly of the distributions we get; as a consequence, all the fission characteristics are also different.

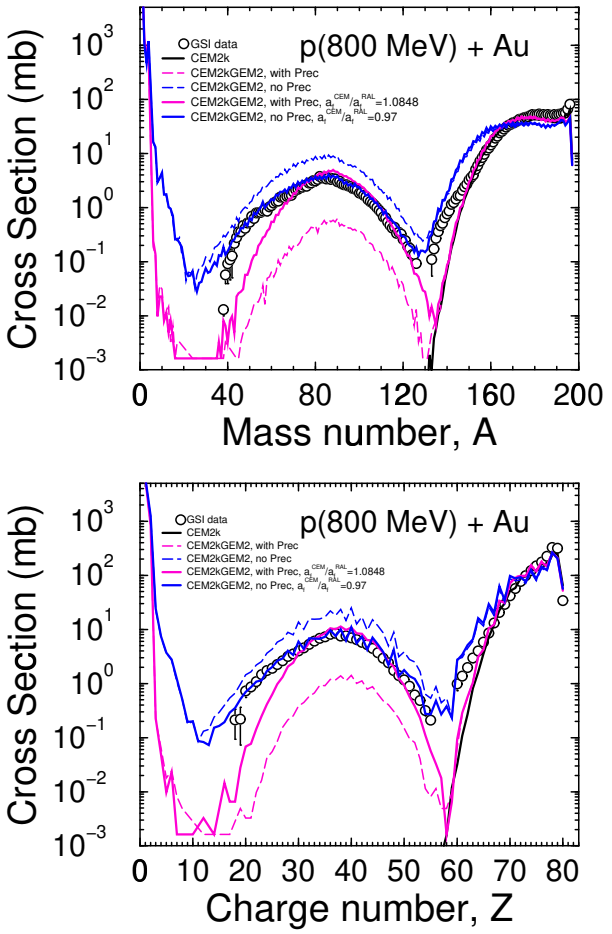

Figure 5. Comparison of the experimental[9] mass and charge distributions of the nuclides produced in the reaction p(800 MeV) + Au (circles) with different calculations. The black solid lines show our calculations with CEM2k without contributions from fission. The dashed red and blue lines show results found by merging CEM2k with GEM2 without any modifications when preequilibrium emission is (red lines) or is not (blue lines) included. Solid color lines show results from CEM2k+GEM2 with a modified a_f: red lines are for the case with preequilibrium emission ($a_f^{CEM}/a_f^{RAL} = 1.0848$) and blues lines show the results without preequilibrium emission ($a_f^{CEM}/a_f^{RAL} = 0.97$).

Furihata used GEM2 coupled either with the Bertini INC[57] or with the ISABEL[58] INC code, which also differs from our INC, and did not include preequilibrium particle emission. Therefore the real fissioning nuclei simulated by Furihata differ from the ones in our simulations, and the parameters adjusted by Furihata to work the best with her INC should not be the best for us. To get a good description of the fission cross section (and fission-fragment yields) we need to modify at least one parameter in GEM2, namely to adjust the level density parameter a_f to get the correct fission cross section (see Eq. (17)), in the case of fissioning nuclei with $Z \leq 88$ (pre-actinides), and the parameter $C(Z)$ (see Eq. (19) and Tab. 5) for fissioning nuclei with $Z > 88$ (actinides). From the dashed lines on Fig. 5 we see that we need to enlarge a_f in our code to get a proper fission cross section when we include preequilibrium emission (the excitation energy of our fissioning nuclei and their A and Z are smaller than provided by the Bertini or ISABEL INC without preequilibrium), and we need to decrease a_f in the case without preequilibrium. By increasing a_f by 1.0848 compared with the original RAL and GEM2 value ($a_f^{CEM}/a_f^{RAL} = 1.0848$), we are able to reproduce correctly the fission cross section when we take into account preequilibrium emission (below, we label such results as "with Prec"). In the case with no preequilibrium emission, a proper fission cross section is obtained for $a_f^{CEM}/a_f^{RAL} = 0.97$ (we label such results as "no Prec"). We choose these values for a_f for all our further calculations of this reaction and do not change any other parameters.

The solid lines in Fig. 5 show results with these values of a_f. One can see that the "no Prec" version provide a good description of both the mass and charge distributions and agrees better with the data for these characteristics than the "with Prec" version (that is not true for isotopic distributions of individual elements, as we show below). The "with Prec" version reproduces correctly the position of the maximum in both A and Z distributions and the yields of fission fragments not too far from these maximums, but the calculated distributions are narrower than the experimental ones. This is again because both Atchison and Furihata fitted their A and Z distributions using models without preequilibrium emission, which provide higher values for the excitation energy, A, and Z of fissioning nuclei. This means that to get a good description of A and Z distributions for fission fragments using GEM2 in CEM2k "with Prec", we would need to modify the A and Z distributions of fission fragments in GEM2 (see Sec. B.2 and B.3), making them wider. This would take us beyond the scope of the present work and here we do not vary any more parameters than we have already discussed.

Fig. 6 shows the GSI measurements[9] of the A and Z distributions of the kinetic energy of products from the same reaction compared with our CEM2k+GEM2 calculations both with and without preequilibrium emission. Both versions of our calculations are in reasonable agreement with the data, with slightly better agreement for the version "no Prec". These results suggest to us that a small adjustment of kinetic-energy distribution parameters in GEM (see Sec. B.4) may be required for a better description of the data with our CEM2k+GEM2 code.

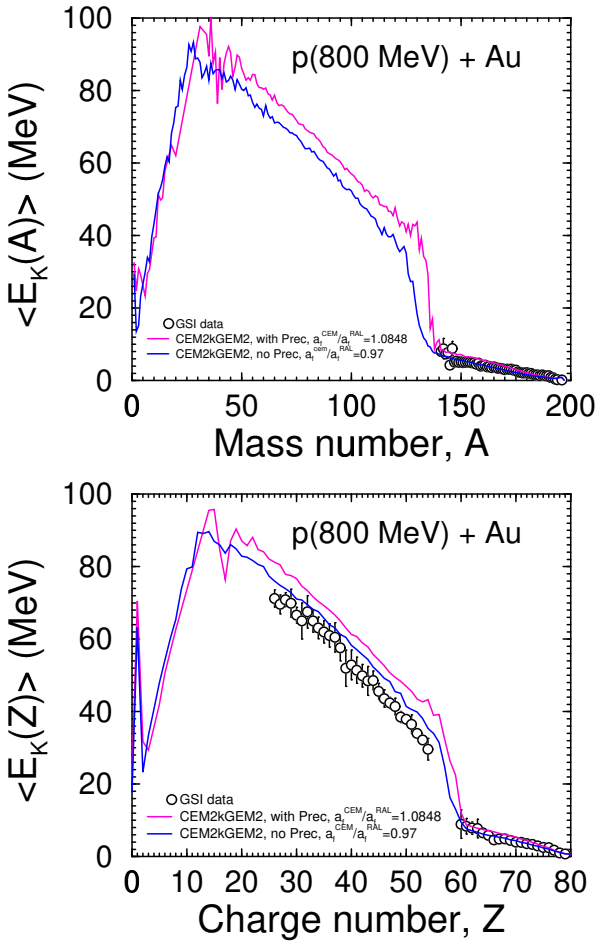

Figure 6. Comparison of the experimental[9] mass and charge distributions of the kinetic energy of the nuclides produced in the reaction p(800 MeV) + Au (circles) with out CEM2k+GEM2 calculations: "with Prec" results are shown by red lines, "no Prec" results are shown by blue lines.

Mass and charge distributions of the yields or kinetic energies of the nuclides produced show only general trends and are not sensitive enough to the details of a reaction. It is much more informative to study the characteristics of individual nuclides and particles produced in a reaction. Fig. 7 shows a comparison of the experimental data on production yields of twelve separate isotopes with Z lying from 20 to 80 from the same reaction measured at GSI[9] with our calculations using both the "with Prec" (upper plot) and "no Prec" (lower plot) versions.

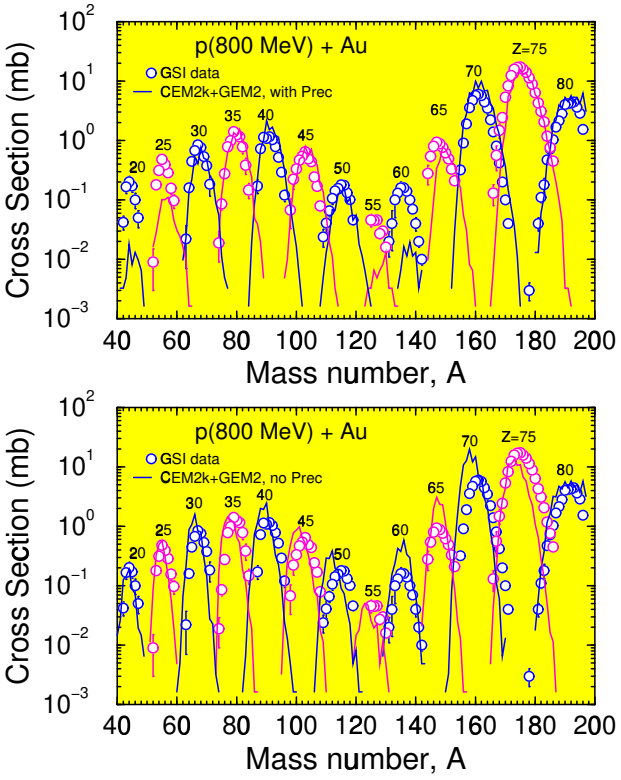

Figure 7. Experimental[9] mass distributions of the cross sections of twelve isotopes with the charge Z from 20 to 80 compared with our CEM2k+GEM2 calculations. "With Prec" results are shown on the upper plot, while "no Prec" results are shown in the lower one.

The agreement (or disagreement) of our calculations with these data is different from what we have for the integral A or Z distributions in Figs. 5 and 6: We see that for the isotopes produced in the spallation region (not too far from the target) and for fission fragments in the region with the maximum yield, the version "with Prec" agree much better with the data than the version "no Prec". Only for production of isotopes at the border between spallation and fission and between fission and fragmentation does the version "with Prec" underestimates the data, due to too narrow A and Z distributions in the simulation of fission fragments, as we discussed previously. The "no Prec" version agrees better with the data in these transition regions but are in worse agreement for isotopes both in the spallation region and in the middle of the fission region. We conclude that if a model agrees well with some A or Z distributions it does not necessarily mean that it also describes well production of separate isotopes. In other words, integral A and Z distributions are not sensitive enough to develop and test such models, a practice which has often used in the literature.

It is more difficult for any model to describe correctly the energy dependence for the production cross sections of different isotopes, *i.e.*, excitation functions. We calculated using both the "with Prec" and "no Prec" versions of CEM2k+GEM2 all the excitation functions for the same reaction, p + Au, for proton energies from 10 MeV to 3 GeV and compared our results

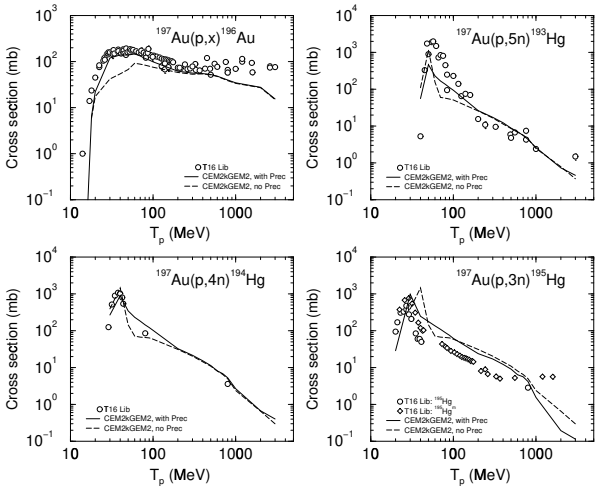

Figure 8. Excitation functions for the production of ^{196}Au, ^{193}Hg, ^{194}Hg, and ^{195}Hg from p+^{197}Au. Results by CEM2k+GEM2 "with Prec" are shown by solid lines and "no Prec" by dashed lines. Experimental data (symbols) are from our LANL compilation (T16 Lib)[59] and are available from the authors upon request.

with all available data from our compilation referred to here as T-16 Library ("T16 Lib")[59]. Only several typical examples from our comparison are shown below. Figs. 8 and 9 show two examples of excitation functions for the production of several isotopes in the spallation region. One can see a not too good but still reasonable agreement of both calculations with the data. Nevertheless, the version "with Prec" reproduces these experimental excitation functions better that the version "no Prec". Similar results were obtained for excitation functions of many other isotopes in the spallation region.

Figs. 10 and 11 show two examples of excitation functions for the production of fission fragments. We see that merging CEM2k with GEM2 allows us to reasonably describe yields of fission fragments, while in the old standard CEM2k we do not have any fission fragments and are not able to describe such reactions at all. We see that as shown in Figs. 5 and 7 for a single proton energy of 800 MeV, the "with Prec" version agrees better with the data in the whole energy region for the production of most of the fission fragments. Only on the border between fission and fragmentation regions (^{54}Mn and ^{60}Co in Fig. 10) does the "no Prec" version agree much better with the data than the "with Prec" version; the reason for this we have already discussed.

In Fig. 12 we show examples of excitation functions for the production of light fragments, in the fragmentation region, that are produced in CEM2k+GEM2 only via evaporation (the contribution to the yield of these isotopes from fission or deep spallation is negligible). We see that with the "no Prec" version, GEM2 reproduces correctly the yields of light fragments ^{7}Be and

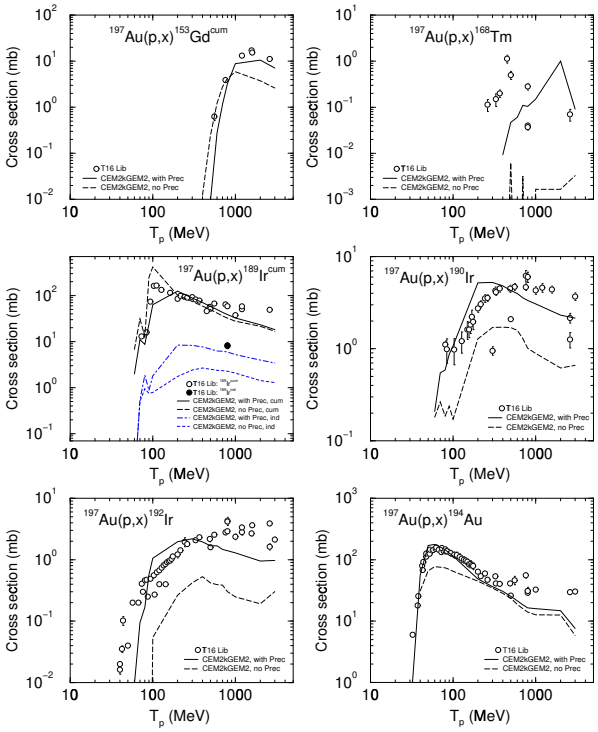

Figure 9. The same as Fig. 8 but for the production of ^{153}Gd^{cum}, ^{168}Tm, ^{189}Ir^{cum}, ^{190}Ir, ^{192}Ir, and ^{194}Au. Note that for ^{153}Gd, only the cumulative yield is shown, where measured and calculated cross sections contain contributions not only from a direct production of ^{153}Gd ("independent yield"), but also from all its decay-chain precursors. For ^{189}Ir, both cumulative and independent cross sections are shown.

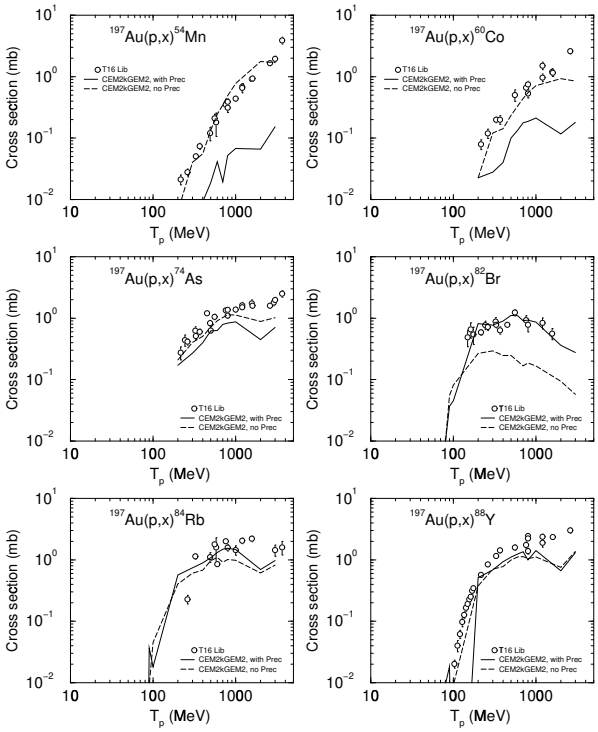

Figure 10. The same as Fig. 8 but for the production of ^{54}Mn, ^{60}Co, ^{74}As, ^{82}Br, ^{84}Rb, and ^{88}Y. Note that while some minor contribution to the production of these isotopes from deep spallation processes may be present, all of them are produced mainly via fission.

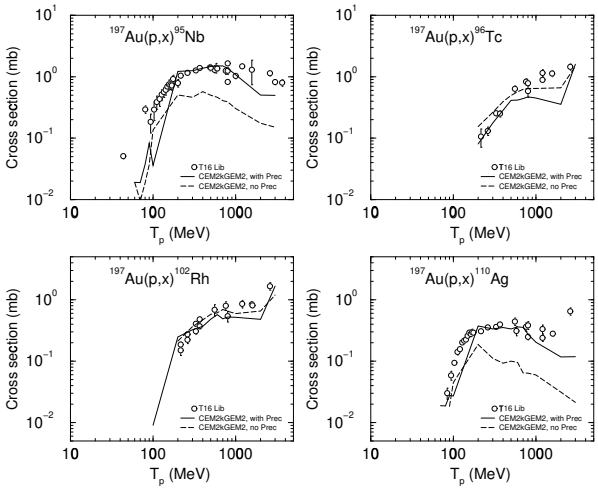

Figure 11. The same as in Fig. 8 but for the production of ^{95}Nb, ^{96}Tc, ^{102}Rh, and ^{110}Ag.

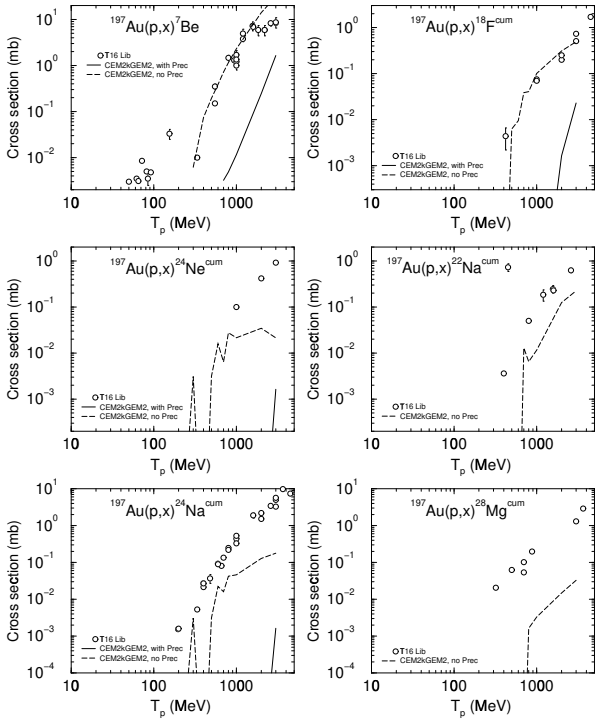

Figure 12. The same as Fig. 8 but for the production of ^{7}Be, ^{18}F^{cum}, ^{24}Ne^{cum}, ^{22}Na^{cum}, ^{24}Na^{cum}, and ^{28}Mg^{cum}. These fragments are produced in CEM2k+GEM2 only via evaporation.

^{18}F, and not so well the excitation functions for heavier fragments ^{22}Na and ^{24}Ne. With increasing mass of the fragment, the calculations progressively underestimate their yields (*e.g.*, for ^{28}Mg, the calculated excitations function is more than an order of magnitude below the data). The version "with Prec" strongly underestimates the yields of all these fragments, and this is again not surprising, as Furihata developed her model and fitted all parameters without taking into account preequilibrium processes. Undeniably, the parameters determining the yields of evaporated fragments in GEM (inverse cross sections and Coulomb barriers) could be adjusted to get a good agreement with the data for the yields of light fragments with the version "with Prec". This is not an aim of our present work and we will not do this here. Even if we were to do this, we expect in advance to get similar results as we got for the "no Prec" version: It would be possible to describe correctly the yields of light fragments but not of heavy fragments like ^{24}Na and ^{28}Mg. To describe such heavy fragments the model would need to be improved further, by considering other mechanisms for heavy fragment production in addition to the evaporation process taken into account by GEM2.

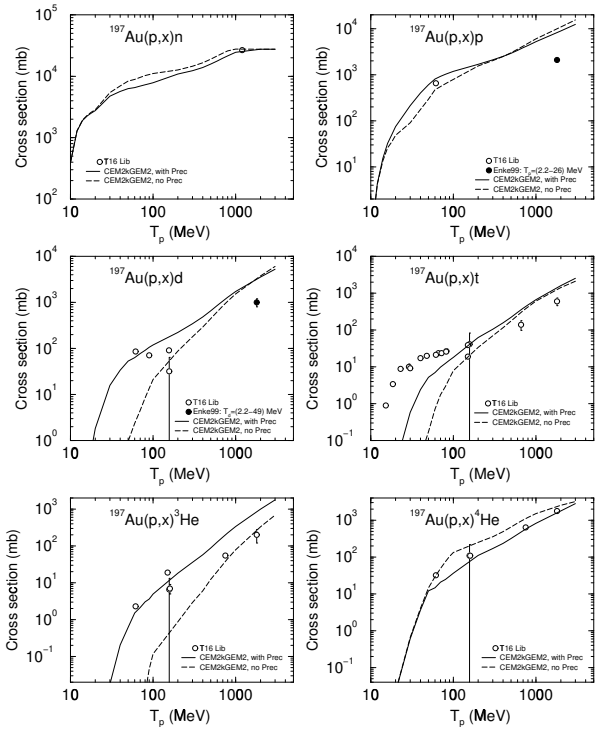

Figure 13. The same as Fig. 8 but for the production of n, p, d, t, ^{3}He, and ^{4}He. The complex particles are produced in CEM2k+GEM2 via evaporation and preequilibrium emission; n and p are also produced during the cascade stage.

Finally, Fig. 13 shows the excitation functions for emission of nucleons and complex particles up to α for this reaction. Note that the data for these excitation functions are not so extensive and precise as we have for heavier products: many data points were obtained by integration (plus extrapolation) of the spectra of particles measured only at several angles and only for a limited range of energy. But even from a comparison with these sparce and imprecise data we see that the "with Prec" version describes these excitation function much better than the "no Prec" version. This is an expected result as the high Coulomb barriers for heavy nuclear targets oppose evaporation of low energy complex particles and the main contribution to their yields comes from preequilibrium emission from highly excited pre-compound nuclei.

Besides yields of reaction products, reliable models should also describe their spectra. Data on particle spectra are important for shielding calculations and other applications, in addition to the scientifc interest in understanding nuclear reactions. For the reaction discussed here, p + Au, there are measurements by Bertrand and Peelle for proton and complex-particle spectra at incident proton energies of 29, 39, and 62 MeV[60]. We compare calculated angle-integrated energy spectra for p, d, t, ^{3}He, and ^{4}He with the data at 62 MeV in Fig. 14.

We see that the "with Prec" version (black solid histograms) describes a good part of the complex particle emission spectra, though the tails of calculated spectra are significantly below the data (we discuss in the next section an attempt to improve the description of complex particle spectra in CEM2k). The "no Prec" version (dashed red and green histograms) fails completely to describe these spectra, as it contains contribution to complex particle emission only from evaporation, and evaporation spectra do not extend significantly above particle energies of 20 MeV. Even in the low-energy evaporation region, the evaporation component for the ^{3}He spectra (shown by a green dashed histogram in Fig. 14) is more than an order of magnitude below the data[60]. Let us mention that this is a problem not only of GEM2 but also for all other similar models where preequilibrium emission is not modeled. What is more, some of the evaporation models used in the literature, like the GSI evaporation model by Schmidt *et al.*[61], which is used in conjunction with the Liege INC by Cugnon *et al.*[15] , evaporate only n, p, and ^{4}He, and do not include evaporation of d, t, and ^{3}He providing for them no yield.

For completeness sake, we show here also an example of results from a calculation with the merged CEM2k+GEM2 code of a reaction on an actinide, p(190 MeV) + ^{232}Th. This reaction was recently measured by Duijvestijn *et al.*[62,63], and at a similar energy of 200 MeV, by Titarenko *et al.*[64] To get for actinides

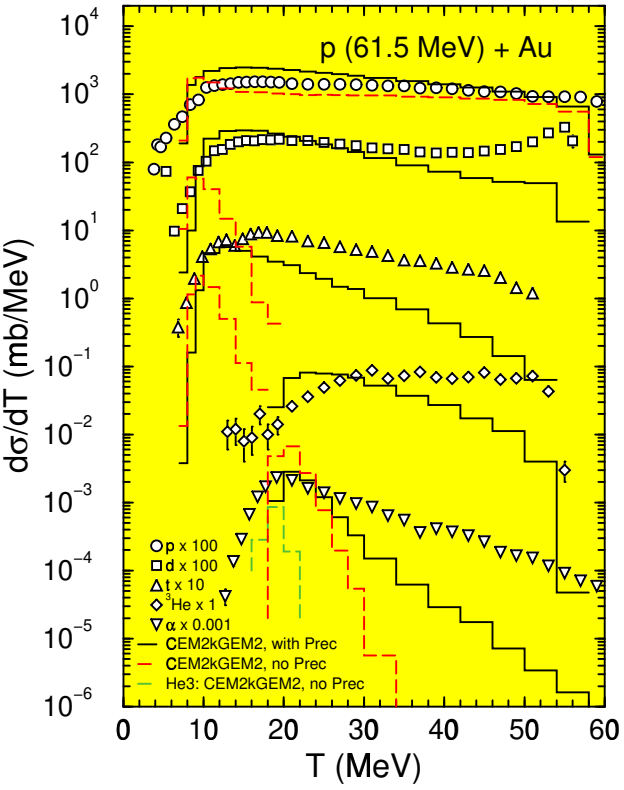

Figure 14. Angle-integrated energy spectra of p, d, t, ^{3}He, and ^{4}He from 61.5 MeV protons on ^{197}Au. Calculations from the merged CEM2k+GEM2 code "with Prec" are shown by solid black histograms and "no Prec", by dashed red (and green, for ^{3}He) histograms. Experimental data (symbols) are from Bertrand and Peelle[60].

a proper fission cross section, we need to adjust in GEM2 the parameters $C(Z)$ (or, also $A_0(Z)$) in Eq. (19), as they were fitted by Atchison to work the best with Bertini's INC and we have in CEM2k our own INC. As mentioned above, for actinides, Eq. (13) is not used in GEM2 and a_f is not used in any calculations, therefore we do not need to adjust a_f/a_n, for fissioning nuclei with $Z > 88$. We found that to get with CEM2k+GEM2 a fission cross section in agreement with the data for our reaction we need to use $C(Z)^{CEM}/C(Z)^{RAL} = 8.50$ for the "with Prec" version and $C(Z)^{CEM}/C(Z)^{RAL} = 1.77$ for "no Prec" (while we use $a_f^{CEM}/a_f^{RAL} = 1.0848$ which we fitted for the reaction p(800 MeV) + Au, "with Prec"). This is the only parameter we fitted for this reaction. Nevertheless, we should mention that for reactions on actinides at intermediate or high energies, the parameter a_f^{CEM}/a_f^{RAL} should also be fitted along with $C(Z)^{CEM}/C(Z)^{RAL}$. In some simulated events several protons can be emitted at the cascade and preequilibrium stages of the reaction, as well as at the evaporation stage, before the compound nucleus actually fissions, and the charge of the fissioning nucleus can have $Z \leq 88$, even when the initial charge of the target has $Z > 88$. At the same time, for $Z \leq 88$, due to charge exchange reactions, the charge of the fissioning nucleus may exceed 88, so that we would need to fit as well $C(Z)^{CEM}/C(Z)^{RAL}$. This is a peculiarity of treating the fission probability P_f differently for the elements above and below $Z = 89$ in the Atchison model.

Fig. 15 shows mass distributions of products from p(190 MeV) + ^{232}Th calculated with both versions of CEM2k+GEM2 compared to the available experimental data[62,64].

We need to mention that these data are not as good for testing and developing models as are the GSI data measured in inverse kinematics for the p + Au reaction discussed above: All the data shown in Fig. 15 were obtained by the γ-spectrometry method. Only some of the produced isotopes were measured, and most of the data were measured for the cumulative yields. To get the "experimental" A-distribution, we summed for each A the available data taking care to not sum the individual cross sections already included in some cumulative yields; but the resulting A-distribution is still not complete, as many isotopes were not measured. This means that some theoretical values can be above the experimental data (where some isotopes were not measured) without necessarily implying disagreement between calculations and measurements. What is more, many of Duijvestijn's data tabulated in[62] differ significantly from the same data tabulated in an earlier publication[63] for some isotopes: *e.g.*, for ^{72}Zn the difference is a factor of 8.03 (!), possibly due to a misprint in[63]. We chose for our comparison Duijvestijn's data

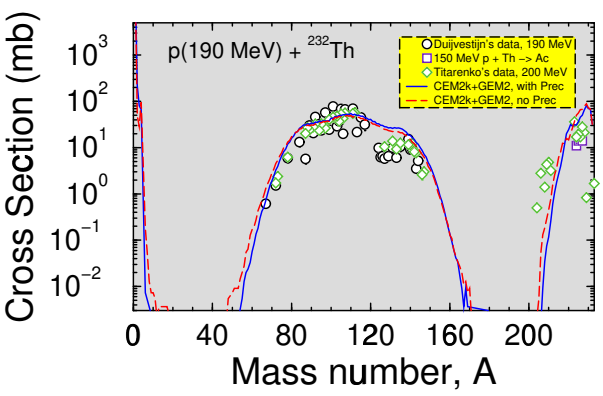

Figure 15. Mass distribution of nuclides from p (190 MeV) + ^{232}Th. The 190 MeV data are from[62]; the 200 MeV data are by Titarenko *et al.*[64]; data for several Ac isotopes from p (150 MeV) + ^{232}Th are from the T-16 compilation[59]. Our "with Prec" results are shown by the solid blue line and the "no Prec" results are shown by the dashed red line.

tabulated in[62] as more reliable than the earlier tabulation published in[63]. (We thank Dr. Duijvestijn for clarifying this point.)

One can see that after the parameter $C(Z)$ is adjusted, both the "with Prec" and "no Prec" versions of CEM2k+GEM2 describe equally well the mass distribution of the products from this reaction; therefore it is not possible to choose between either of the versions from a comparison with these not very informative data. It is more useful to compare calculations with the yields of individually measured isotopes. In Fig. 16, we compare our calculations with all cross sections measured by Duijvestijn[62] for each nuclide separately, where we can compare our results with the data (we do not include in our comparison the nuclides measured only either in their isomer or ground states, as our model does not provide such information: CEM2k+GEM2 provides only yields for the sum of isotope production cross sections both in their ground and excited states). We see that on the whole, the "with Prec" version agrees better with most of the individually measured cross sections than the "no Prec" version and for many of the measured isotopes the disagreement is less than a factor of two. Nevertheless, for several isotopes like ^{72}Ga, ^{96}Tc, and ^{124}I, we see some big disagreements. For comparison, we also show in Fig. 16 calculations by the phenomenological code YIELDX of Silberberg, Tsao, and Barghouty[23] and with the phenomenological code CYF by Wahl[65] often used in applications. We see that both these phenomenological systematics completely fail to describe the production of all isotopes from this reaction, indicating that we cannot rely on phenomenological systematics and must develop reliable models to be used in applications. We note that the agreement of our CEM2k+GEM2 re-

sults with the measured product yields is different for different reactions. So, in Ref.[56], for the reaction p (100 MeV) + ^{238}U, we got an almost perfect agreement of calculations with the data: for this particular reaction, both "with Prec" and "no Prec" results by CEM2k+GEM2 almost coincide with the available data (see details in Ref.[56]).

To summarize this section, merging CEM2k with GEM2 allows us to describe reasonably well many fission and fragmentation reactions in addition to the spallation reactions already described well by CEM2k. Some reactions, like production of fission fragments at the borders between fission and fragmentation or between fission and emission of heavy fragments like Na and Mg are poorly described by CEM2k+GEM2 in its current version. This disagreement does not discourage us; the results of the present work suggest that some of the fission and evaporation parameters of GEM2 can be adjusted to get a much better description of all reactions. This lends credibility to such an approach. There is one more drawback of this approach to be mentioned: considering evaporation of up to 66 particles in GEM becomes extremely time consuming when calculating reactions with heavy targets at high incident energies. But even this disadvantage may be mitigated by the performance of modern computers. We have nevertheless some more serious doubts about the current version of GEM2 related to its lack of self-consistency, *e.g.*:

1) using different, not physically related parameterizations for inverse cross sections and Coulomb barriers for different particles and fragments;

2) using different level density parameters for the same compound nuclei when calculating evaporation and estimating fission probability from the widths of neutron evaporation and fission;

3) different, and purely phenomenological treatments of fission for pre-actinide and actinide nuclei;

4) not taking into account at all the angular momentum of compound and fissioning nuclei;

5) rough estimations for the fission barriers and level density parameters, *etc.*

This means that an approach like GEM2 can in principle be used to describe fission and evaporation of particles and fragments heavier that ^{4}He after the INC and preequilibrium parts of CEM2k and other models, but it should be considerably improved striving first to progressively incorporate better physics, and only after that looking on agreement with the data.

The results of the present work and from[56] show that on the whole, the merged CEM2k+GEM2 code agrees better with most of tested experimental data when we take into account the preequilibrium emission of particles, than when we neglect completely preequilibrium processes. But there is still an open question to be solved here; we have had some indications for many years that CEM accounts for too many

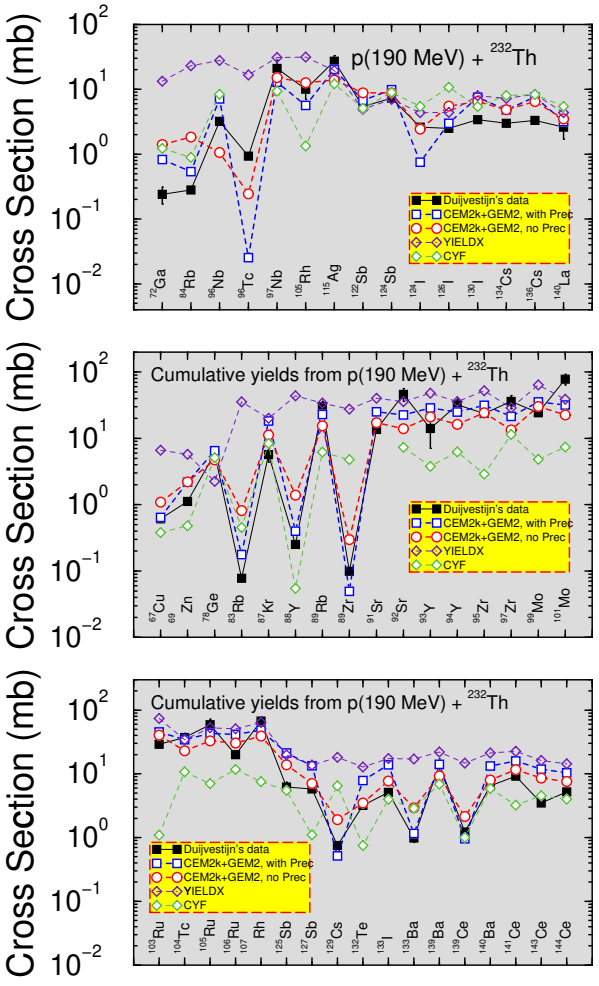

Figure 16. Detailed comparison between experimental[62] (black filled squares) and calculated cross sections of individual (upper plot) and cumulative (middle and bottom plots) reaction products. Our CEM2k+GEM2 "with Prec" results are shown by connected blue squares and the "no Prec" results are shown by connected red circles. For comparison, predictions by the phenomenological systematics YIELDX of Silberberg, Tsao, and Barghouty[23] are shown by connected indigo diamonds, and results calculated by Dr. W. B. Wilson with the phenomenological code CYF by Wahl[65] are shown with connected green diamonds. We thank Dr. Wilson for providing us with results of his calculations with the CYF code included in this figure.

preequilibrium particles, at least at energies above the pion-production threshold. To solve this problem, as a "zero-step" approximation, in our original CEM2k version[10] we neglected in the exciton model the transitions that decrease or do not change the number of excitons $\Delta_n = -2$ and $\Delta_n = 0$, shortening in this way the preequilibrium stage of reactions. We do not like this approach as it is arbitrary, "ad hoc", even though this "never come back" approximation is used in some popular codes[14,66]. In the present work we removed this arbitrary condition in CEM2k and the "with Prec" version takes into account all the preequilibrium transitions $\Delta_n = +2$, 0, and -2, making the preequilibrium stage of a reaction longer and increasing the number of emitted preequilibrium particles. The results of the present work indicate to us once again that we need to take into account the preequilibrium stage in reactions, but we need less particle emission than we currently calculate at this stage. In[56], we explore an alternative way to shorten the preequilibrium particle emission in CEM, based on Ref. [67], but this work is incomplete so we do not include these results here.

IV. EXTENSION OF CEM2K

In this section we present an alternative way of describing fission-fragment, complex-particle and light-fragment emission with CEM2k, by extending and developing further our model itself, without using independent evaporation models developed by other authors.

One of the unsolved problems in all versions of the CEM code is using the Dostrovsky *et. al.*[39] approximations for the inverse cross sections (Eq. (2) with the parameters shown in Tab. 3) both for preequilibrium and evaporation. As already mentioned, the Dostrovsky *et. al.*[39] formula is simple and allows one to calculate the integral in Eq. (1) analytically. This is the main reason we have kept Dostrovsky's formula in all our previous versions of the CEM code, even though we know it is not reliable enough. We develop and incorporate into CEM2k our own approximation for inverse cross sections. As a first step, we collected experimental data on absorption or fusion cross sections for all target nuclei and for all particles and fragments for which we were able to find data, *i.e.*, just the "inverse" cross sections when we deal with particle emission. Then, we collected from the literature theoretical estimations and systematics for the inverse cross sections and compared these systematics with the data to find which systematics better describe the data. An example from this study is shown in Fig. 17, where we compare available data on inverse cross sections for n, p, d, t, ^{3}He, and ^{4}He on ^{27}Al with the approximation from Ref.[39], NASA systematics by Tripathi, Cucinota, and Wilson[33], a parameterization by Kalbach[34], an approximation by Tang, Srinivasan, and Azziz[69], and the results calculated with the phenomenological code CROSEC by Barashenkov and Polanski[70]. Similar figures have been plotted for other target nuclei for which we were able to find experimental data. One can see a big disagreement between Dostrovsky *et al.*'s[39] approximation and the data.

Probably, the reason why Dostrovsky *et. al.*'s[39] formula works quite well in many evaporation models to describe emission of neutrons and protons from many reactions is because it overestimates both and in similar ways the neutron and proton inverse cross sections (correspondingly, their width Γ_n and Γ_p) at energies above about 20 MeV. The emission of n and p are the main channels of most evaporation processes, and emission of particles are simulated in evaporation codes using only the ratios $\Gamma_j / \sum_j \Gamma_j$ but not the absolute values of particle widths, Γ_j. Dostrovsky formula underestimates significantly the inverse cross sections for the complex particles, and this is one of the reasons why all evaporation models that use Dostrovsky's formula underestimate the yields of complex particles. An additional problem introduced by the overestimation of the nucleon emission probabilities occurs when fission is considered. A realistic value of the fission barrier and the saddle-point level density will give too small a fission probability when compared to a too-large nucleon evaporation probability. This then leads to the empirical determination of unphysically large values of the level density parameter, *etc.*

From Fig. 17 and similar figures for other nuclei which we have made, we determined that the overall best agreement with experimental data is achieved with the NASA systematics by Tripathi, Cucinota, and Wilson[33]; therefore we chose it as the basis to calculate inverse cross sections in CEM2k. Nevertheless, this systematics does not reproduce correctly the inverse cross sections for neutrons at energies below about 10 MeV. We address this problem the following way: We calculate with the NASA systematics[33] the inverse cross sections for all charged particles and for neutrons with energies above T_n^{max}, where a maximum in the neutron inverse cross section is predicted by[33], and with the systematics by Kalbach[34], for neutrons with energies below T_n^{max}. We tabulated the values of T_n^{max} for each nucleus and renormalize the neutron inverse cross sections calculated with the systematics by Kalbach[34] so that they coincide at T_n^{max} with the NASA values[33], providing a continuity of the neutron inverse cross sections at this energy.

A detailed description of the NASA and Kalbach systematics may be found in[33,34] and references therein. For completeness sake, we outline here only their basic ideas and formulas.

The NASA systematics[33] is a universal parameterization for any systems of colliding nuclei, therefore can be used to calculate inverse cross sections not only

for nucleons and complex particles but also for heavier fragments. It uses the following form for the reaction cross sections (inverse cross sections, in our case):

$$\sigma_R = \pi r_0^2 (A_P^{1/3} + A_T^{1/3} + \delta_E)^2 (1 - V_C/E_{cm}), \quad (28)$$

where A_P and A_T are the projectile and target mass numbers, respectively, $r_0 = 1.1$ fm is energy independent, E_{cm} is the total center-of-mass kinetic energy in MeV, δ_E is an energy dependent parameter described below, and V_C [MeV] is the energy-dependent Coulomb barrier defined as:

$$V_C = 1.44 Z_P Z_T / R. \quad (29)$$

Here,

$$R = r_P + r_T + 1.2(A_P^{1/3} + A_T^{1/3})/E_{cm}^{1/3}, \quad (30)$$

with $(i = P, T)$

$$r_i = 1.29 (r_i)_{rms}, \quad (31)$$

with the root-mean-square radius, $(r_i)_{rms}$, obtained directly from experimental data.

There is an energy dependence in the reaction cross section at intermediate and higher energies mainly due to two effects—transparency and Pauli blocking. This is taken into account in δ_E which is given by

$$\delta_E = 1.85S + 0.16\frac{S}{E_{cm}^{1/3}} - C_E + 0.91\frac{(A_T - 2Z_T)Z_P}{A_T A_P}, \quad (32)$$

where S is the mass asymmetry term and is given by

$$S = A_P^{1/3} A_T^{1/3} / (A_P^{1/3} + A_T^{1/3}) \quad (33)$$

and is related to the volume overlap of the collision system. The last term on the right hand side of Eq. (32) accounts for the isotopic dependence of the reaction cross section.

The term C_E is related to the transparency and Pauli blocking and is given by

$$C_E = D\,(1 - \exp(-E/40)) - 0.292 \exp(-E/792) \times \cos(0.229 E^{0.453}). \quad (34)$$

Here D is related to the density dependence of the colliding system scaled with respect to the density of the C+C system, *i.e.*:

$$D = 1.75(\rho_{A_P} + \rho_{A_T})/(\rho_{A_C} + \rho_{A_C}). \quad (35)$$

The density of a nucleus is calculated in the sharp-surfaced sphere model and for a nucleus of mass A_i is given by

$$\rho_{A_i} = A_i / \frac{4}{3}\pi r_i^3, \quad (36)$$

where the radius of the nucleus r_i is defined in Eq. (31). The physics related to the constant D is to simulate the modifications of the reaction cross sections due to Pauli blocking. This effect helps present a universal picture of the reaction cross section[33].

At lower energies (below several tens of MeV) where the overlap of interacting nuclei is small (and where the Coulomb interaction modifies the reaction cross section significantly) the modifications of the cross sections due to Pauli blocking are small, and gradually play an increasing role as the energy increases, since this leads to higher densities where Pauli blocking gets increasingly important. For proton-nucleus interactions, where there is not much compression effect, a single constant value of $D = 2.05$ gives good results for all proton-nucleus collisions. For alpha-nucleus collisions, where there is a little compression, the best value of D is given by[33]

$$D = 2.77 - 8.0 \times 10^{-3} A_T + 1.8 \times 10^{-5} A_T^2 - 0.8/(1 + \exp(250 - E)/75). \quad (37)$$

For lithium nuclei because of the "halos", compression is less and hence the Pauli blocking effect is less important and a reduced value of $D/3$ gives better results for the reaction cross sections at the intermediate and higher energies.

Note that for proton-nucleus collisions this method of calculating the Coulomb energy underestimates its value for the very light closed shell nuclei of alpha and carbon, and these should be increased by a factor of 27 and 3.5 respectively for a better fit[33].

Kalbach's approximation for inverse cross sections[34] is based on optical-model reaction cross sections using an empirical parameterization of Chatterjee, Murthy, and Gupta[73] fitted for different particles using different optical potentials, with some additional modifications and described in[34]. For instance, the reaction cross section σ_R (inverse cross section, in our case) for neutrons (used here) is written as

$$\sigma_R = \lambda\epsilon + \mu + \nu/\epsilon, \quad (38)$$

where λ, μ, ν are mass-dependent parameters and ϵ is the neutron laboratory energy in MeV. As mentioned in[73], the addition of the linear term $\lambda\epsilon$ in Eq. (38) greatly improves the fit as compared with the Dostrovsky *et al.* approximation[39]. Separating out the energy dependence as in Eq. (38), the dependence of λ, μ, ν on target mass number A, was obtained empirically as[73]:

$$\begin{aligned} \lambda &= \lambda_0 A^{-1/3} + \lambda_1, \\ \mu &= \mu_0 A^{1/3} + \mu_1 A^{2/3}, \\ \nu &= \nu_0 A^{4/3} + \nu_1 A^{2/3} + \nu_2. \end{aligned} \quad (39)$$

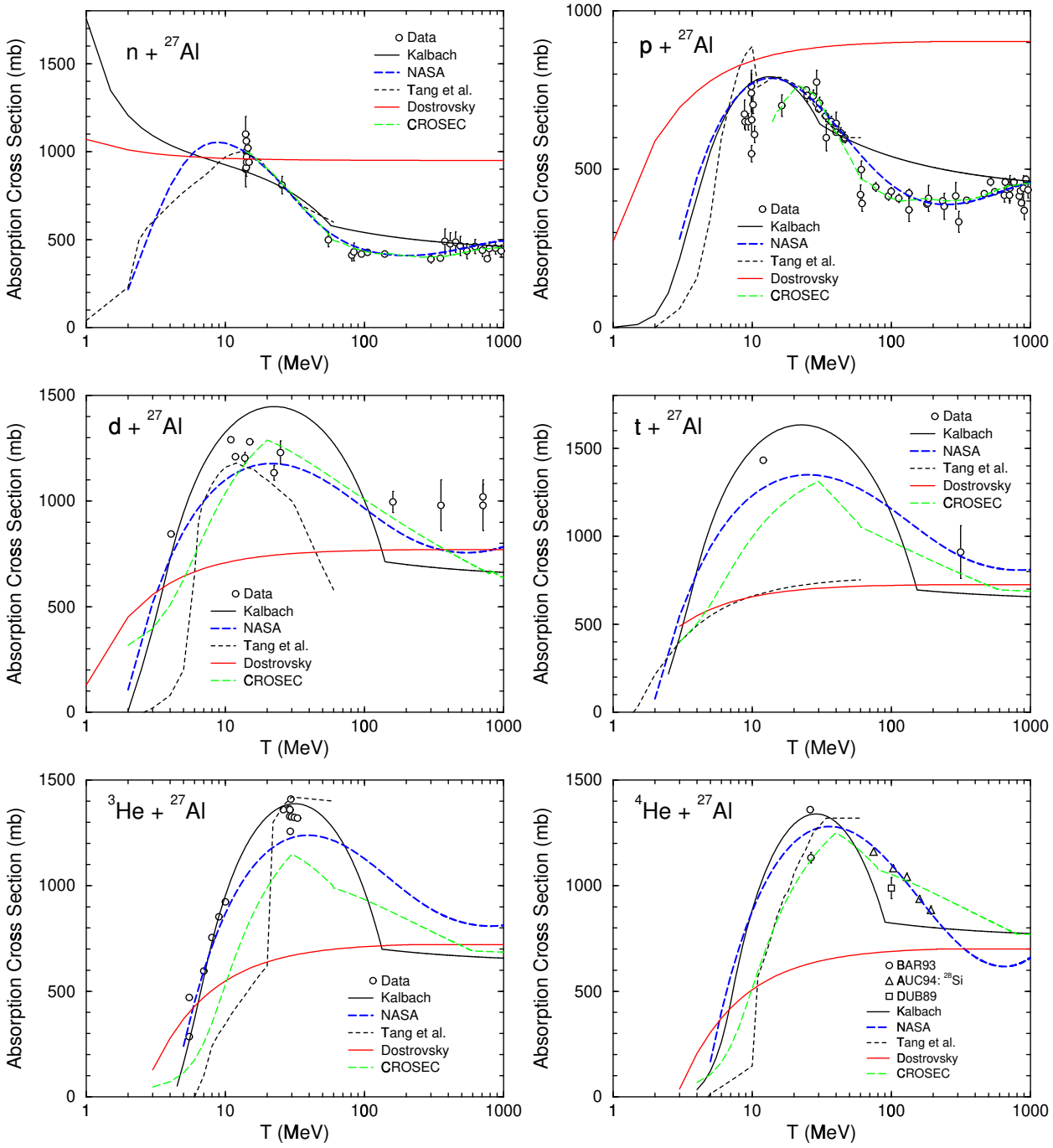

Figure 17. Comparison of experimental data on absorption cross sections for n, p, d, t, ^{3}He, and ^{4}He on ^{27}Al with the Dostrovsky *et. al.*[39] approximation, the NASA systematics by Tripathi, Cucinota, and Wilson[33], a parameterization by Kalbach[34], an approximation by Tang, Srinivasan, and Azziz[69], and results calculated with the phenomenological code CROSEC by Barashenkov and Polanski[70]. Most of the data points (circles, either without a special label or labeled as "BAR93") shown here are from the compilation by Barashenkov[35]; several data points are by Auce *et al.*[71] (triangles labeled as "AUC94"), and a data point for ^{4}He is measured by Dubar *et al.*[72] (the square labeled as "DUB89").

The seven parameters λ_0, λ_1, μ_0, μ_1, ν_0, ν_1, and ν_2 in Eq. (39) were fitted and tabulated by Chatterjee, Murthy, and Gupta[73] for different optical potentials (for different incident particles from n up to α), with a priority to the potential by Mani *et al.*[74] for neutrons. In 1982, the original[73] neutron parameterization was modified by S. K. Gupta to include an effective barrier of 2.4 MeV (see details in[34]), and is now used in the Kalbach approximation for neutron inverse cross sections[34] with the following values (different from the ones of Ref.[73]) for the parameters in Eq. (38): $\lambda_0 = 12.10$, $\lambda_1 = -11.27$, $\mu_0 = 234.1$, $\mu_1 = 38.26$, $\nu_0 = 1.55$, $\nu_1 = -106.1$, and $\nu_2 = 1280.8$. In addition, Kalbach has changed somehow arbitrarily[34] the neutron "barrier" from 2.4 MeV to 0.5 MeV to raise the neutron emission cross section for emission energies below about 1.5 MeV. Also, after the choice of the neutron potential of Mani *et al.*[74] was made in 1963, new data became available, and the earlier comparisons with measured non-elastic cross sections have been extended to include additional targets. This led to a normalization factor for the parameterized optical model cross section having the form[34]:

$$R_n(A) = \begin{cases} 0.7 + 0.3A/40 & \text{for } A < 40 \ , \\ 1.0 & \text{for } A \geq 40 \ . \end{cases} \qquad (40)$$

Thus, the current version of the Kalbach approximation for neutron inverse cross sections used here reads like $\sigma_{inv} = \sigma_R \times R_n(A)$ with σ_R and $R_n(A)$ defined by Eqs. (38–40) and the seven parameters listed above.

An example of inverse cross sections calculated with our method compared to experimental data for n, p, d, t, ^{3}He, and ^{4}He on ^{12}C, ^{40}Ca, ^{56}Fe, and ^{238}U is shown in Fig. 18.

For comparison, calculations using the NASA systematics by Tripathi, Cucinota, and Wilson[33], the Kalbach parameterization[34], and the Dostrovsky *et. al.*[39] approximation are shown as well. One can see that our hybrid approach combining the NASA systematics by Tripathi, Cucinota, and Wilson[33] and the Kalbach parameterization[34] reproduces well the measured inverse cross sections for n, p, d, t, ^{3}He, and ^{4}He and agrees much better with the data than the approximation by Dostrovsky *et. al.*[39] used earlier in all versions of our CEM code. Similar results are obtained for other nuclear targets for which we found data.

We incorporated this hybrid approximation for σ_{inv} in our CEM2k code and use it to calculate inverse cross sections for all particles to be evaporated from a compound nucleus or emitted at the preequilibrium stage of a reaction. The widths for particle emission, Γ_j, are calculated by integrating Eq. (1) (and a similar equation for preequilibrium particles; see details in[68]) numerically.

To be able to describe production of light fragments heavier than ^{4}He, as a first step, we extended the evaporation process including emission of up to 66 different particles, the same considered by Furihata in GEM2 and listed in Tab. 1. Following Furihata, we consider evaporation of fragments both in the ground and excited states, and calculate the widths for the emission of excited fragments and their energy in the same manner as realized in GEM2 by Furihata and described above in Sec. III.A.

We enlarged the number of fragments that may be emitted at the preequilibrium stage, considering the possibility of emission of up to 29 different preequilibrium particles and fragments (the first 29 from Tab. 1, those having $Z \leq 6$).

As we use now in CEM2k the Tripathi, Cucinota, and Wilson systematics[33] for charged-particle inverse cross sections that employ the energy dependent approximation for the Coulomb barriers defined by Eqs. (29–31), we replaced the old routine that calculates Coulomb barriers according to Dostrovsky *et. al.*[39] used in all previous versions of CEM code with a new routine that calculates Coulomb barriers using Eqs. (29–31). We did this for self-consistency of the model: we use the same approximation for Coulomb barriers while calculating inverse cross sections and in all other parts of the code where Coulomb barriers are used.

In this extended version of the CEM2k, we consider also the possibility of "creating" high-energy d, t, ^{3}He, and ^{4}He by final state interactions among emitted cascade nucleons outside of the target, using the coalescence model as implemented by Gudima *et al.*[75] In contrast to most other coalescence models for heavy-ion induced reactions, where complex-particle spectra are estimated simply by convolving the measured or calculated inclusive spectra of nucleons with corresponding fitted coefficients (see, *e.g.*[76], and references therein), CEM2k uses in its simulation of particle coalescence real information about all emitted cascade nucleons and does not use integrated spectra. CEM2k assumes that all the cascade nucleons having differences in their momenta smaller than p_c and a correct isotopic content form an appropriate composite particle. This means that the formation probability for, *e.g.*, a deuteron is

$$W_d(\vec{p},t) = \int\int d\vec{p}_p\, d\vec{p}_n\, \rho^C(\vec{p}_p,t)\rho^C(\vec{p}_n,t) \times \delta(\vec{p}_p + \vec{p}_n - \vec{p})\Theta(p_c - |\vec{p}^{\,c.m.} - \vec{n}^{c.m.}|), \qquad (41)$$

where the particle density in momentum space is related to the one-particle distribution function f by

$$\rho^C(\vec{p},t) = \int d\vec{r} f^C(\vec{r},\vec{p},t). \qquad (42)$$

Here, the superscript C shows that only cascade nucleons are taken into account for the coalescence process.

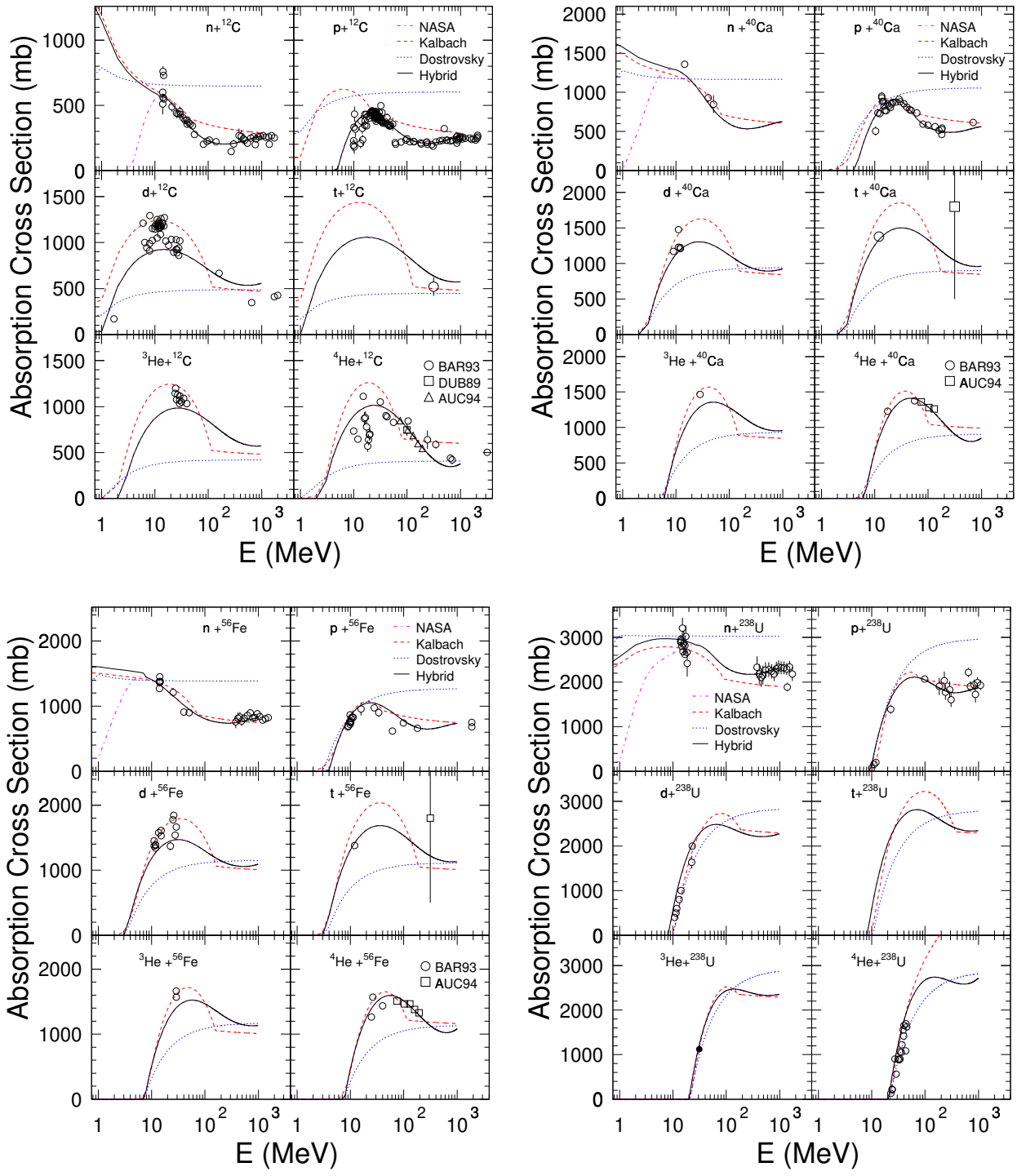

Figure 18. Inverse cross sections for n, p, d, t, ^{3}He, and ^{4}He on ^{12}C, ^{40}Ca, ^{56}Fe, and ^{238}U calculated with our routine HYBRID (black solid lines) compared with available experimental data (symbols) from the compilation by Barashenkov[35] (circles, either without a special label or labeled as "BAR93"), by Auce *et al.*[71] (labeled as "AUC94"), and by Dubar *et al.*[72] (labeled as "DUB89"). For comparison, calculations using the NASA systematics by Tripathi, Cucinota, and Wilson[33] are shown by magenta dot-dashed lines, results from the Kalbach parameterization[34] are shown with red dashed lines, and predictions by the Dostrovsky *et. al.*[39] approximation are shown by blue dotted lines.

The coalescence radii p_c were fitted for each composite particle in Ref.[75] to describe available data for the reaction Ne+U at 1.04 GeV/nucleon, but the fitted values turned out to be quite universal and were subsequently found to satisfactorily describe high-energy complex-particle production for a variety of reactions induced both by protons and nuclei at incident energies up to about 200 GeV/nucleon. These parameters used in the present version of CEM2k are:

$$\begin{aligned} p_c(\mathrm{d}) &= 90 \text{ MeV/c}, \\ p_c(\mathrm{t}) = p_c(^3\mathrm{H}e) &= 108 \text{ MeV/c}, \\ p_c(^4\mathrm{H}e) &= 115 \text{ MeV/c}. \end{aligned} \tag{43}$$

If several cascade nucleons are chosen to coalesce into composite particles, they are removed from the status of nucleons and do not contribute further to such nucleon characteristics as spectra, multiplicities, *etc.*

To describe fission-fragment production from heavy fissioning compound nuclei, we incorporated into the present version of CEM2k the thermodynamical fission model by Stepanov[77] with its own parameterizations for mass and charge widths, level-density parameters, fission barriers, *etc.* The already extended length of the current paper does not allow us to present here details of the thermodynamical fission model by Stepanov[77] and sample results obtained with it. We plan to publish our fission results in a separate paper; for the moment, we only note that this model statistical by nature and coupled with CEM2k it provides similar results to those we got with the modified RAL model from GEM2, with some better agreement with the data for pre-actinides and some worse agreement for actinides.

For brevity, we call the extended version of CEM2k described here as CEM2k2f (shorthand for "second fission model") and show below several results on complex-particle and fragment emission from several reactions, referring to them as from CEM2k2f.

Fig. 19 shows examples of angle-integrated energy spectra of p, d, t, ^{3}He, and ^{4}He from 62 MeV proton interactions with Al, ^{56}Fe, Y, and ^{120}Sn calculated with CEM2k2f (red histograms) compared with experimental data by Bertrand and Peelle[60] (symbols). For comparison, results obtained with previous versions of CEM are shown with black histograms, namely: calculations with CEM95[2] for ^{56}Fe, Y, and ^{120}Sn, and with CEM97[3] for Al. We still have some problems in a correct description of the high-energy tails of complex-particle spectra (that is probably related to direct processes of complex particle production like knock-out and pick-up which are not included in CEM2k2f), although the improved CEM2k2f provides a much better agreement with the data than the older versions CEM95 and CEM97.

The new inverse cross sections and Coulomb barriers implemented here provide a correct and better description of the evaporation parts of particle spectra, but require an adjustment of the "condensation" probability γ_j at the preequilibrium stage of reactions (see details in[1,68]). CEM assumes[1] that during the preequilibrium part of a reaction p_j excited particles (excitons) are able to condense with probability γ_j forming a complex particle which can be emitted during the preequilibrium state. In our first publication on CEM[1], γ_j was roughly estimated as

$$\gamma_j \simeq p_j^3 (p_j/A)^{p_j - 1}, \tag{44}$$

(A is the mass number of the pre-compound nucleus before emitting the particle j), and this estimation was used in all the succeeding versions of CEM. Generally, γ_j is a parameter of the preequilibrium model, and in the literature it is taken from fitting the theoretical preequilibrium spectra to the experimental ones, which gives rise to an additional, as compared to (44), dependence of the factor γ_j on p_j, mass-number A, and excitation energy (see, *e.g.* Ref.[78]). Our calculations show that one may obtain a reasonable description with CEM2k2f of all complex particles up to ^{4}He from many reactions if we use values for γ_j estimated using Eq. (44) divided by 3 for d and t, and by 4 for ^{3}He. The results shown in Fig. 19 are obtained with this estimation for γ_j. It is clear that if we fit γ_j for each particle and each reaction as done in Ref.[78], one may obtain a much better agreement with the data, but such exercises are outside the aim of our work. Our calculations of several reactions show that if we were to fit γ_j in CEM2k+GEM2, we could also obtain a much better description of complex particle spectra than the one shown in Fig. 14, but such a fit is as well beyond the aim of the present work.

All spectra of particles from Al, ^{56}Fe, and ^{120}Sn shown on Fig. 19 are calculated without introducing a coalescence mechanism for complex-particle production. This is because for proton-induced reactions at these incident energies the multiplicity of fast nucleons emitted at the cascade stage of reactions is so small that the role of coalescence of complex particles from such nucleons is negligible. As an example, in Fig. 19 we show only for Y (by blue histograms) calculated spectra that contain contributions from coalescence production of complex particles. One can see that indeed the contribution from the coalescence mechanism is very small for this reaction and complex particle spectra calculated with and without this mechanism almost coincide.

Another example of the role of different mechanisms of particle production from these reactions is shown in Table 6, where we present the mean total multiplicities of complex particles from Y and ^{120}Sn calculated by CEM2k2f (last column) together with their contributions from preequilibrium, evaporation, and coalescence reaction mechanisms (third to fifth columns).

Table 6. Role of different CEM2k2f reaction mechanisms in complex particle production (multiplicities) from p (62 MeV) + Y and ^{120}Sn

Nucleus	Ejectile	Prec	Evap	Coales	Total
^{89}Y	d	2.96e-2	1.41e-3	1.83e-3	3.28e-2
	t	5.34e-3	1.13e-4	5.66e-6	5.46e-3
	^{3}He	1.92e-3	1.13e-5	2.83e-6	1.94e-3
	^{4}He	4.19e-2	1.56e-2	–	5.75e-2
^{120}Sn	d	3.17e-2	6.51e-4	1.75e-3	3.41e-2
	t	8.58e-3	1.57e-4	–	8.74e-3
	^{3}He	7.59e-4	–	–	7.59e-4
	^{4}He	3.15e-2	6.19e-3	–	3.77e-2

The percentage of the coalescence mechanism to the total complex particle yields is only 5.6% for d from Y and 5.1% for d from ^{120}Sn, while for t and ^{3}He from Y is only of the order of 0.1% and below the statistical errors of these reactions as simulated by CEM2k2f for ^{4}He from Y and t, ^{3}He, and ^{4}He from ^{120}Sn. Nevertheless, our other studies show that at high incident energies[79,80] and for heavy-ion induced reactions[75], the coalescence mechanism of complex-particle production is important and often is the main mechanism of high-energy complex particle production; therefore we incorporate this mode into CEM2k2f.

It is informative to observe from Table 6 that due to high Coulomb barriers for complex particles from medium and heavy nuclei, the main contribution to production of such particles comes from preequilibrium emission, while the evaporation mode is less important for such reactions.

Fig. 20 shows examples of ^{3}He and ^{4}He double-differential spectra from interaction of 300 and 480 MeV protons with Ag calculated with CEM2k2f compared with experimental data by Green and Korteling[81]. One can see that CEM2k2f reproduces reasonably these data though it overestimates most of the spectra, especially the high-energy tails of them. Probably, by fitting γ_j for this reactions as discussed above one may obtain a much better agreement with the measurement, but we didn't do any additional fitting of γ_j for these reactions. We also see some problems with a correct description of angular distributions of ^{3}He and ^{4}He from these reactions and we plan to address this point in our further work. These results are preliminary and though we did not get a very good agreement with the data, they are encouraging to us as they help us to clarify ways of further improving CEM2k.

From Fig. 20 we conclude that we probably get with CEM2k2f too much preequilibrium particle emission from these reactions. Such a conclusion may also be drawn from the results presented in Table 7, where we present a comparison of the total total yields of several particles and light fragments from 480 MeV p + Ag calculated with CEM2k2f with experimental data by Green, Korteling, and Jackson[82]. The results presented in Table 7 are preliminary, without any additional fitting of any parameters of CEM2k2f, nevertheless we see a reasonable agreement with the measurement not only for production of ^{3}He and ^{4}He, but also for heavier fragments. We calculated this reaction with CEM2k2f both including preequilibrium-particle emission (third column in Table 7) and ignoring it (last column in Table 7). We can see that for many of the fragment-production cross sections (^{8}Li, ^{9}Li, ^{7}Be, ^{9}Be, and ^{11}Be shown in the table) the experimental yields are higher than the ones calculated without preequilibrium emission, and lower than those with preequilibrium emission. Though these results are preliminary and will change when we develop further our model, they may serve as a rough indication that in the present version of CEM2k2f we have too much preequilibrium particle emission, just as we got with CEM2k+GEM2 discussed in Sec. III. We recall again that in[56] we address this point both in our CEM2k[10] and LAQGSM[79] codes merged with GEM2[37,38] using an approach based on Ref.[67], and the results obtained there are promising.

Table 7. Comparison of the measured[82] total production cross sections (mb) for several ejectiles from 480 MeV p + Ag with our preliminary CEM2k2f results with and without preequilibrium emission

Ejectile	Exp. data	CEM2k2f with Prec	CEM2k2f no Prec
n	–	3.97e+3	4.50e+3
p	–	9.30e+2	9.94e+2
d	–	2.85e+2	3.51e+2
t	–	1.27e+2	1.35e+2
^{3}He	3.42e+1	3.98e+1	3.02e+1
^{4}He	4.44e+2	7.68e+2	1.11e+3
^{6}He	–	6.60e+0	3.61e+0
^{8}He	–	1.31e-1	1.61e-2
^{6}Li	3.67e+1	9.91e-2	9.28e+0
^{7}Li	4.20e+1	3.59e-2	5.27e+0
^{8}Li	4.48e-1	1.24e-3	5.31e-1
^{9}Li	6.98e-2	1.08e-4	8.37e-2
^{7}Be	8.36e-1	5.85e-3	1.20e+0
^{9}Be	9.22e-1	1.06e-2	1.73e+0
^{10}Be	4.16e-1	6.23e-4	1.52e-1
^{11}Be	1.29e-2	2.24e-5	1.66e-2
^{12}Be	–	7.65e-7	1.02e-3
^{8}B	–	5.98e-5	3.46e-2
^{10}B	4.85e-1	1.35e-3	4.22e-1

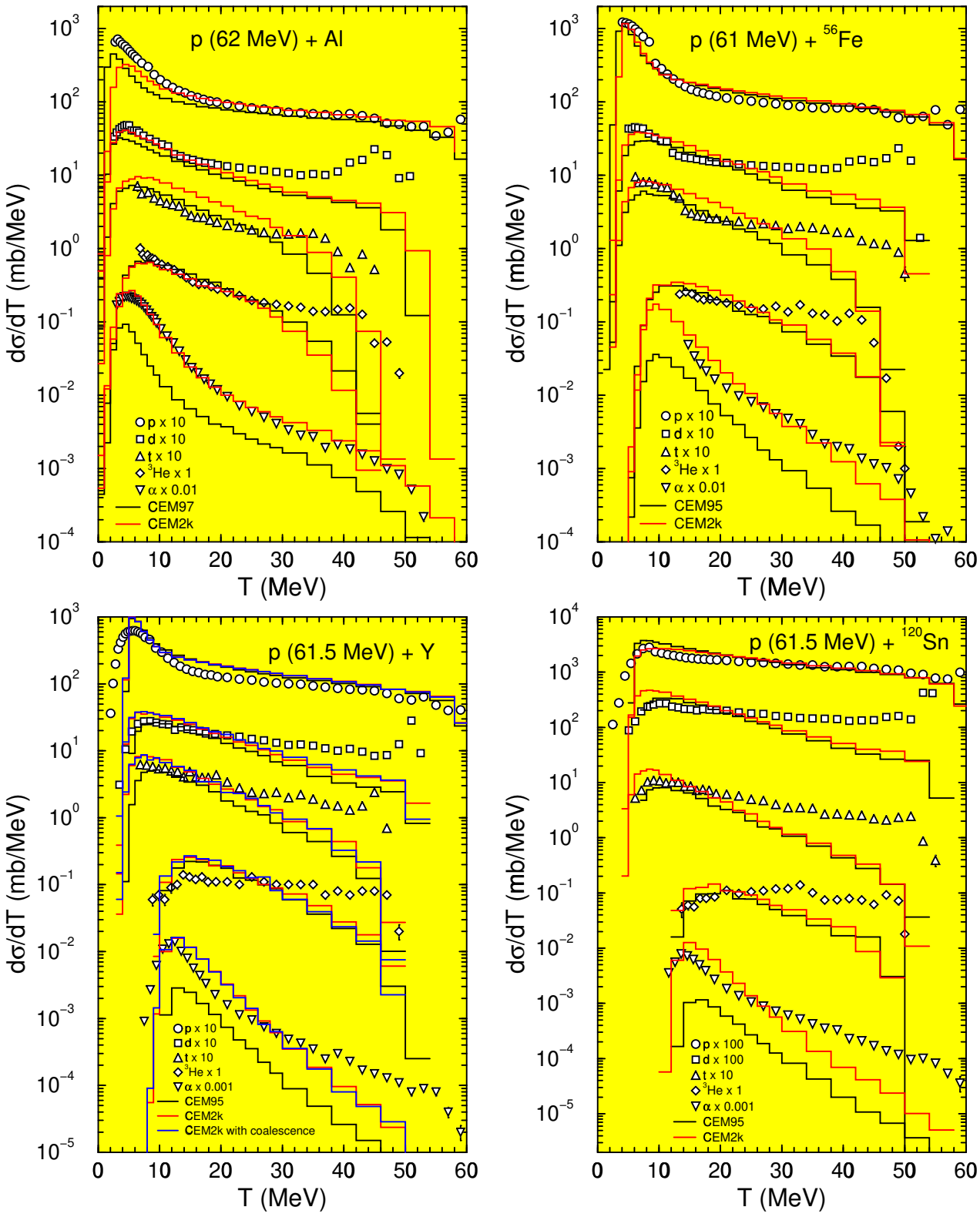

Figure 19. Angle-integrated energy spectra of p, d, t, ^{3}He, and ^{4}He from 62 MeV protons on Al, ^{56}Fe, Y, and ^{120}Sn. Calculations from the CEM2k2f code are shown by red histograms and from CEM95[2] (for ^{56}Fe, Y, and ^{120}Sn) and CEM97[3] (for Al) are shown by black histograms. For Y, the blue histograms show CEM2k2f results taking into account contributions from coalescence of complex particles from fast cascade nucleons, as described in the text. Experimental data (symbols) are by Bertrand and Peelle[60].

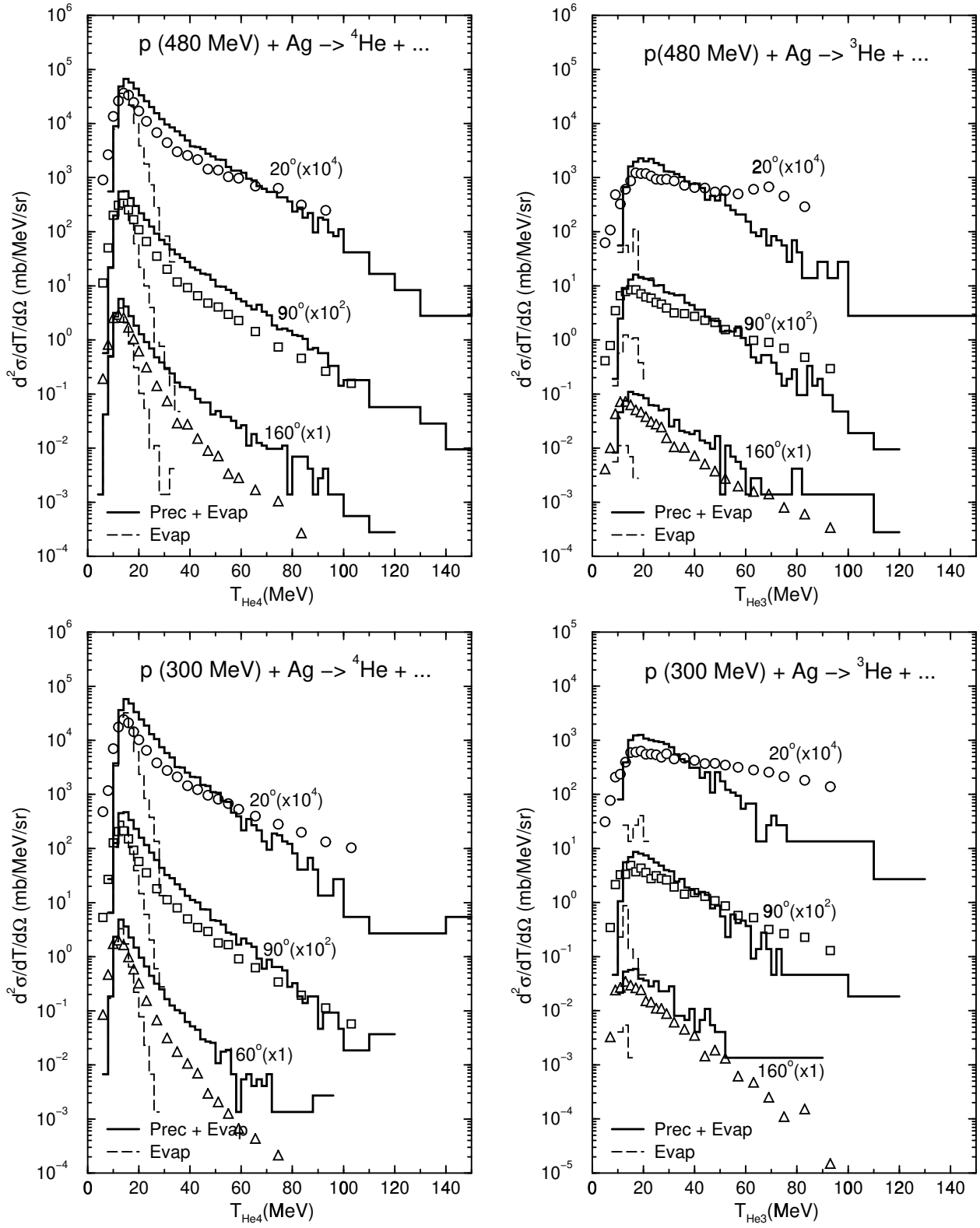

Figure 20. Double-differential spectra of ^{4}He and ^{3}He from 480 and 300 MeV protons on Ag. Calculations from the CEM2k2f code are shown by solid histograms and contribution from only the evaporation mode, by dashed histograms. Experimental data (symbols) are by Green and Korteling[81].

Finally, we have investigated the well known code GEMINI by Charity[83] as an alternative way to describe production of various fragments by merging GEMINI with both our CEM2k and LAQGSM. The preliminary results we find for spallation, fission, and fragmentation products from several reactions are promising and we will present our results from this study in a separate paper.

V. FUTURE WORK

The two modifications of the CEM2k model presented here allow us to describe satisfactorily many fission and fragmentation reactions in addition to the spallation reactions which are already quite well described by CEM2k.

Our results presented in Sec. III show that the Generalized Evaporation Model code GEM2 by Furihata is a useful tool and when merged with CEM2k (or LAQGSM) it allows us to reproduce a large variety of fission and fragmentation measurements, though some tuning of several GEM2 parameters will be required. We may choose a model similar to GEM2 in our codes to describe fission, fragmentation, and evaporation yields, but it must be significantly extended and improved in order to properly describe complex particles, light and heavy fragments not produced in fission, and more importantly, to become self-consistent and better grounded from a physical point of view.

The latest version of CEM2k described in Sec. IV, CEM2k2f, contains new inverse cross sections and Coulomb barriers, new routines to calculate widths of emitted particles and to simulate their kinetic energies using arbitrary approximations for the inverse cross sections and Coulomb barriers, allows evaporation of up to 66 different particles both in the ground and excited states and emission of up to 29 different preequilibrium particles, takes into account coalescence of complex particles from fast nucleons emitted at the cascade stage, and describes much better complex-particle spectra and yields than its precursors.

Our work is not finished yet. For example, at the evaporation and preequilibrium stages we still need to make an "ad hoc" decision about how many different particles should be included into consideration so that we have production of light fragments heavier than ^{4}He but maintain the running time of the code at a reasonable level. Our new algorithms and routines do not impose any limitations to the energy dependence of the particle emission probabilities, and we plan to try to improve the present description of the level densities and particle emission widths with a hope to describe better the tails of complex-particle spectra.

We consider also implementation into CEM2k a model of fragmentation, to be able to describe emission of fragments like Na, Mg, and heavier, and possibly, incorporation of the Fermi break-up model to replace the preequilibrium and evaporation models when the residual excited nucleus after the cascade stage of a reaction is very light.

Our work on fission in CEM2k is also not finished. For instance, we are not satisfied with the situation that in both the improved versions of the CEM2k discussed here we still have an additional input parameter to describe fission cross sections: either $C(Z)$, in the GEM2/RAL approach for nuclei with $Z > 88$, and/or a_f/a_n, in the same model for lighter fissioning nuclei with $Z \leq 88$ and when using the model by Stepanov. In addition, to get with CEM2k a better description of fission-fragment distributions, the approximations used in both GEM/RAL and Stepanov's fission models to simulate A, Z, and kinetic-energy distributions for fission fragments should be further adjusted in our code.

We emphasize that it is not sufficient to analyze only A and Z distributions of the product yields when evaluating the type of model discussed here, as is often done in the literature, but that it is essential to study all the separate isotope yields as well as the spectra of light particles and fragments. This should be done for different target nuclei, different incident particles, and at different energies.

ACKNOWLEDGMENTS

We thank Dr. Shiori Furihata for several useful discussions, for sending us her Generalized Evaporation Model code GEM, and providing us further with its updated version, GEM2. We thank Dr. Nikita Stepanov for providing us with his thermodynamical fission model implemented in the ITEP code INUCL and useful explanations on his code. We thank Prof. Barashenkov and Dr. Polanski for providing us with their phenomenological code CROSEC and Dr. Tsao for providing our colleagues with his and Dr. Silberberg's phenomenological code YIELDX we used here and in our other works. We are grateful to Drs. M. B. Chadwick, R. E. Prael, D. D. Strottman, L. S. Waters, and W. B. Wilson for useful discussions, interest, and support.

This study was supported by the U. S. Department of Energy and by the Moldovan-U. S. Bilateral Grants Program, CRDF Project MP2-3025.

REFERENCES

1. K. K. Gudima, S. G. Mashnik, and V. D. Toneev, "Cascade-Exciton Model of Nuclear Reactions," *Nucl. Phys.* **A401**, 329–361 (1983).

2. S. G. Mashnik, "User Manual for the Code CEM95," JINR, Dubna (1995); OECD NEA Data Bank, Paris, France (1995);
http://www.nea.fr/abs/html/iaea1247.html;
RSIC-PSR-357, Oak Ridge, 1995.

3. S. G. Mashnik and A. J. Sierk, "Improved Cascade-Exciton Model of Nuclear Reactions," *Proc. Fourth*

Workshop on Simulating Accelerator Radiation Environments (SARE4), Knoxville, TN, USA, September 14–16, 1998, pp. 29–51, T. A. Gabriel, Ed., ORNL, Oak Ridge (1999).

4. A. J. Sierk and S. G. Mashnik, "Modeling Fission in the Cascade-Exciton Model," *Proc. Fourth Workshop on Simulating Accelerator Radiation Environments (SARE4)*, Knoxville, TN, USA, September 14–16, 1998, pp. 53–67, T. A. Gabriel, Ed., ORNL, Oak Ridge (1999).

5. *MCNPX^{TM} User's Manual, Version 2.1.5*, edited by Laurie S. Waters, Los Alamos National Laboratory Report LA-UR-99-6058, Los Alamos (1999).

6. W. Wlazlo *et al.*, "Cross Sections of Spallation Residues Produced in 1A GeV ^{208}Pb on Proton Reactions," *Phys. Rev. Lett.* **84**, 5736–5739 (2000).

7. T. Enqvist *et al.*, "Isotopic Yields and Kinematic Energies of Primary Residues in 1A GeV ^{208}Pb + p Reactions," *Nucl. Phys.* **A686**, 481–524 (2001).

8. J. Taieb *et al.*, "Measurement of ^{238}U Spallation Product Cross Sections at 1 GeV per Nucleon," http://www-wnt.gsi.de/kschmidt/publica.htm#Conferences.

9. F. Rejmund *et al.*, "Measurement of Isotopic Cross Sections of Spallation Residues in 800 A MeV ^{197}Au + p Collisions," *Nucl. Phys.* **A683**, 540–565 (2001); J. Benlliure *et al.*, "Isotopic Production Cross Sections of Fission Residues in ^{197}Au-on-proton Collisions at 800 A MeV," *Nucl. Phys.* **A683**, 513–539 (2001).

10. S. G. Mashnik and A. J. Sierk, "CEM2k—Recent Developments in CEM," *Proc. AccApp00, November 13–15, 2000, Washington, DC, USA*, pp. 328–341, American Nuclear Society, La Grange Park, IL, USA, (2001); http://xxx.lanl.gov/ps/nucl-th/0011064.

11. Stepan G. Mashnik and Arnold J. Sierk, "Recent Developments of the Cascade-Exciton Model of Nuclear Reactions," *Proc. Int. Conf. on Nuclear Data for Science and Technology (ND2001), Oct. 7–12, 2001, Tsukuba, Japan*; http://lib-www.lanl.gov/la-pubs/0081526.pdf, to be published in *Journal of Nuclear Science and Technology (2002)*.

12. F. Atchison, "Spallation and Fission in Heavy Metal Nuclei under Medium Energy Proton Bombardment," in *Proc. Meeting on Targets for Neutron Beam Spallation Source, Julich, June 11–12, 1979*, pp. 17–46, G. S. Bauer, Ed., Jul-Conf-34, Kernforschungsanlage Julich GmbH, Germany (1980).

13. F. Atchison, "A Treatment of Fission for HETC," in *Intermediate Energy Nuclear Data: Models and Codes*, pp. 199–218, Proc. of a Specialists's Meeting, May 30–June 1, 1994, Issy-Les-Moulineaux, France, OECD, Paris, France (1994).

14. R. E. Prael and H. Lichtenstein, "User Guide to LCS: The LAHET Code System," LANL Report No. LA-UR-89-3014, Los Alamos (1989); http://www-xdiv.lanl.gov/XTM/lcs/lahet-doc.html.

15. J. Cugnon, C. Volant, and S. Vuillier, "Improved Intranuclear Cascade Model for Nucleon-Nucleus Interactions, *Nucl. Phys.* **A620**, 475–509, (1997).

16. S. G. Mashnik, R. J. Peterson, A. J. Sierk, and M. R. Braunstein, "Pion-Induced Transport of π Mesons in Nuclei," *Phys. Rev. C* **61**, 034601 (2000).

17. A. V. Prokofiev, S. G. Mashnik, and A. J. Sierk, "Cascade-Exciton Model Analysis of Nucleon-Induced Fission Cross Sections of Lead and Bismuth at Energies from 45 to 500 MeV," *Nucl. Sci. Eng.* **131**, 78–95, (1999).

18. G. Audi and A. H. Wapstra, "The 1995 Update to the Atomic Mass Evaluation," *Nucl. Phys.* **A595**, 409–480 (1995).

19. P. Möller, J. R. Nix, W. D. Myers, and W. J. Swiatecki, "Nuclear Ground-States Masses and Deformations," *Atomic Data and Nuclear Data Tables*, **59**, 185–383 (1995).

20. P. Möller, J. R. Nix, and K.-L. Kratz, "Nuclear Properties for Astrophysical and Radioactive-Ion-Beam Application," *Atomic Data and Nuclear Data Tables* **66**, 131–345 (1997).

21. A. V. Ignatyuk *et al.*, "Fission of Pre-Actinide Nuclei. Excitation Functions for the (α, f) Reactions," *Yad. Fiz.* **21**, 1185–1205 (1975) [*Sov. J. Nucl. Phys.* **21**, 612–621 (1975)].

22. A. S. Iljinov *et al.*, "Decay Width and Lifetimes of Excited Nuclei," *Nucl. Phys.* **A543**, 517–557 (1992).

23. R. Silberberg, C. H. Tsao, and A. F. Barghouty, "Updated Partial Cross Sections of Proton-Nucleus Reactions," *Astrophys. J.* **501**, Part 1, 911–819 (1998).

24. J.-J. Gaimard and K.-H. Schmidt, "A Reexamination of the Abrasion-Ablation Model for the Description of the Nuclear Fragmentation Reaction," *Nucl. Phys.* **A531**, 709–745 (1991).

25. A. V. Ignatyuk, N. T. Kulagin, V. P. Lunev, and K.-H. Schmidt, "Analysis of Spallation Residues within the Intranuclear Cascade Model," *Proc. XV Workshop on Phys. of Nucl. Fission, Oct. 3–6, 2000, Obninsk, Russia*; http://www-wnt.gsi.de/kschmidt/publica.htm.

26. S. G. Mashnik *et al.*, "Benchmarking Ten Codes Against the Recent GSI Measurements of the Nuclide Yields from ^{208}Pb, ^{197}Au, and ^{238}U + p Reactions at 1 GeV/nucleon," *Proc. Int. Conf. on Nuclear Data*

for Science and Technology (ND2001), Oct. 7–12, 2001, Tsukuba, Japan; http://lib-www.lanl.gov/la-pubs/0081527.pdf, to be published in *Journal of Nuclear Science and Technology (2002)*.

27. T. W. Armstrong and K. C. Chandler, "HETC A High Energy Transport Code," *Nucl. Sci. Eng.* **49**, 110–111 (1972).

28. V. S. Barashenkov *et al.*, "CASCADE Program Complex for Monte Carlo Simulations of Nuclear Processes Initiated by High-Energy Particles and Nuclei in Gaseous and Condensed Matter," JINR Report R2-85-173, Dubna, 1985; V. S. Barashenkov, F. G. Zheregi, and Zh. Zh. Musul'manbekov, "The Cascade Mechanism of Inelastic Interactions of High-Energy Nuclei," *Yad. Fiz.* **39**, 1133–1134 (1984) [*Sov. J. Nucl. Phys.* **39**, 715–716 (1984)]; V. S. Barashenkov, B. F. Kostenko, and A. M. Zadorogny, "Time-Dependent Intranuclear Cascade Model," *Nucl. Phys.* **A338**, 413–420 (1980).

29. V. S. Barashenkov, A. Yu. Konobeev, Yu. A. Korovin, and V. N. Sosnin, "CASCADE/INPE Code System," *Atomnaya Energiya* **87**, 283–286 (1999) [*Atomic Energy* **87**, 742–744 (1999)].

30. G. A. Lobov, N. V. Stepanov, A. A. Sibirtsev, and Yu. V. Trebukhovskii, "Statistical Simulation of Hadron and Light-Nuclei Interactions with Nuclei. Intranuclear Cascade Model." Institute for Theoretical and Experimental Physics (ITEP) Preprint No. ITEP-91, Moscow, 1983

31. Yu. E. Titarenko *et al.*, "Cross Sections for Nuclide Production in 1 GeV Proton-Irradiated Pb", *Phys. Rev. C* **65**, 064610 (2002).

32. K. Ishibashi *et al.*, "Measurement of Neutron-Production Double-Differential Cross Sections for Nuclear Spallation Reaction Induced by 0.8, 1.5 and 3.0 GeV Protons," *J. Nucl. Sci. Techn.* **34**, 529–537 (1997).

33. R. K. Tripathi, F. A. Cucinotta, and J. W. Wilson, "Accurate Universal Parameterization of Absorption Cross Sections," *Nucl. Instr. Meth. Phys. Res.* **B117**, 347–349 (1996).

34. C. Kalbach, "Towards a Global Exciton Model; Lessons at 14 MeV," *J. Phys. G: Nucl. Part. Phys.* **24**, 847–866 (1998).

35. V. S. Barashenkov, *Cross Sections of Interactions of Particles and Nuclei with Nuclei*, JINR, Dubna, Russia (1993); tabulated data are available from the NEA/OECD Data Bank Web site at http://www.nea.fr/html/dbdata/bara.html.

36. M. Blann, "New Precompound Decay Model," *Phys. Rev. C* **54**, 1341–1349 (1996); M. Blann and M. B. Chadwick, "New Precompound Decay Model: Angular Distributions," *Phys. Rev. C* **57**, 233–243 (1998).

37. S. Furihata, "Statistical Analysis of Light Fragment Production from Medium Energy Proton-Induced Reactions," *Nucl. Instr. Meth. in Phys. Research* **B171**, 252–258 (2000); "The Gem Code—The Generalized Evaporation Model and the Fission Model," *Proc. of Monte Carlo 2000 Conference, October 23–26, 2000, Lisbon, Portugal*, to be published by Springer Verlag; "The Gem Code Version 2 Users Manual," Mitsubishi Research Institute, Inc., Tokyo, Japan (November 8, 2001).

38. Shiori Furihata *et al.*, "The Gem Code—A simulation Program for the Evaporation and Fission Process of an Excited Nucleus," JAERI-Data/Code 2001-015, JAERI, Tokai-mura, Naka-gam, Ibaraki-ken, Japan (2001).

39. I. Dostrovsky, Z. Frankel, and G. Friedlander, "Monte Carlo Calculations of Nuclear Evaporation Processes. III. Application to Low-Energy Reactions," *Phys. Rev.* **116**, 683–702 (1959).

40. V. F. Weisskopf and D. H. Ewing, "On the Yield of Nuclear Reactions with Heavy Elements," *Phys. Rev.* **57**, 472–485 (1940).

41. P. E. Haustein, "An Overview of the 1986–1987 Atomic Mass Predictions," *Atomic Data and Nuclear Data Tables* **39**, 185–393 (1988).

42. A. G. W. Cameron, "A Revised Semiempirical Atomic Mass Formula," *Can. J. Phys.* **35**, 1021–1032 (1957).

43. T. Matsuse, A. Arima, and S. M. Lee, "Critical Distance in Fusion Reactions," *Phys. Rev. C* **26**, 2338–2341 (1982).

44. Shiori Furihata and Takashi Nakamura, "Calculation of Nuclide Productions from Proton Induced Reactions on Heavy Targets with INC/GEM," *Proc. Int. Conf. on Nuclear Data for Science and Technology (ND2001), Oct. 7–12, 2001, Tsukuba, Japan*, to be published in *Journal of Nuclear Science and Technology (2002)*.

45. A. S. Botvina *et al.*, "Statistical Simulation of the Break-up of Highly Excited Nuclei," *Nucl Phys.* **A475**, 663–686 (1987)

46. A. Gilbert and A. G. W. Cameron, "A Composite Nuclear-Level Density Formula with Shell Corrections," *Can. J. Phys.* **43**, 1446–1496 (1965).

47. J. L. Cook, H. Ferguson, and A. R. del Musgrove, "Nuclear Level Densities in Intermediate and Heavy Nuclei," *Australian Journal of Physics* **20**, 477–487 (1967).

48. William A. Friedman and William G. Lynch, "Statistical Formalism for Particle Emission," *Phys. Rev. C* **28**, 16–23 (1983).

49. The Evaluated Nuclear Structure Data File (ENSDF) maintained by the National Nuclear Data Center (NNDC), Brookhaven National Laboratory, http://www.nndc.bnl.gov/.

50. Robert Vandenbosch and John R. Huizenga, *Nuclear Fission*, Academic Press, New York (1973).

51. E. F. Neuzil and A. W. Fairhall, "Fission Product Yields in Helium Ion-Induced Fission of Au^{197}, Pb^{204}, and Pb^{206} Targets," Phys. Rev. **129**, 2705–2710 (1963).

52. A. Ya. Rusanov, M. G. Itkis, and V. N. Okolovich, "Features of Mass Distributions of Hot Rotating Nuclei," *Yad. Fiz.* **60**, 773–803 (1997) [*Phys. At. Nucl.* **60**, 683–712 (1997)]; M. G. Itkis *et al.*, "Fission of Excited Nuclei with Z^2/A =20–33: Mass-Energy Distributions of Fragments, Angular Momentum, and Liquid-Drop Model," *Yad. Fiz.* **58**, 2140–2165 (1995) [*Phys. At. Nucl.* **58**, 2026–2051 (1995)].

53. W. D. Myers and W. J. Swiatecki, "Thomas-Fermi Fission Barriers," *Phys. Rev. C* **60**, 014606 (1999).

54. M. G. Itkis *et al.*, "Experimental Study of the Mass and Energy Distributions of Fragments from Fission," *Ya. Fiz.* **52**, 23–35 (1990) [*Sov. J. Nucl. Phys.* **52**, 15–22 (1990)].

55. F. Atchison, "A Revised Calculational Model for Fission," Paul Scherrer Insititut Report No. 98-12, Villigen PSI (1998).

56. S. G. Mashnik, K. K. Gudima, and A. J. Sierk, "Merging the CEM2k and LAQGSM Codes with GEM2 to Describe Fission and Light-Fragment Production," *Proc. 6th Intl. Workshop on Shielding Aspects of Accelerators, Targets and Irradiated Facilities (SATIF-6), April 10–12, 2002, SLAC, Menlo Park, CA 94025, USA*; http://www.nea.fr/html/science/satif/satif6t2.html.

57. H. W. Bertini, "Low-Energy Intranuclear Cascade Calculation," *Phys. Rev.* **131**, 1801–1871 (1963); "Intranuclear Cascade Calculation of the Secondary Nucleon Spectra from Nucleon-Nucleus Interactions in the Energy Range 340 to 2900 MeV and Comparison with Experiment," *Phys. Rev.* **188**, 1711–1730 (1969).

58. Y. Yariv and Z. Frankel, "Intranuclear Cascade Calculation of High-Energy Heavy-Ion Interactions," *Phys. Rev. C* **20**, 2227–2243 (1979); "Inclusive Cascade Calculation of High Energy Heavy Ion Collisions: Effect of Interactions between Cascade Particles," *Phys. Rev. C* **24**, 488–494 (1981).

59. S. G. Mashnik, A. J. Sierk, K. A. Van Riper, and W. B. Wilson, "Production and Validation of Isotope Production Cross Section Libraries for Neutrons and Protons to 1.7 GeV," *Proc. Fourth Workshop on Simulating Accelerator Radiation Environments (SARE4)*, Knoxville, TN, USA, September 14–16, 1998, pp. 29–51, T. A. Gabriel, Ed., ORNL, Oak Ridge (1999); Eprint: **nucl-th/9812071**; our compilation (T-16 Lib) is permanently updated as new data become available to us.

60. F. E. Bertrand and R. W. Peelle, "Complete Hydrogen and Helium Particle Spectra from 30 to 60 MeV Proton Bombardment on Nuclei with A = 12 to 209 and Comparison with the Intranuclear Cascade Model", *Phys. Rev. C* **8**, 1045–1064 (1973).

61. A. R. Junghans *et al.*, "Projectile-Fragment Yields as a Probe for the Collective Enhancement in the Nuclear Level Density," *Nucl. Phys.* **A629**, 635–655 (1998).

62. Marieke Duijvestijn, *Nucleon-Induced Fission at Intermediate Energies*," PhD thesis, NRG Petten, The Netherlands (2000).

63. M. C. Duijvestijn *et al.*, "Proton-Induced Fission at 190 MeV of ^{nat}W, ^{197}Au, ^{nat}Pb, ^{208}Pb, and ^{232}Th," *Phys. Rev. C* **59**, 776–788 (1999).

64. Yury E. Titarenko *et al.*, "Experimental and Theoretical Study of the Yields of Radionuclides Produced in 232-Th Thin Targets Irradiated by 100 and 800 MeV Protons", *Proc. 3rd Int. Conf. on Accelerator Driven Transmutation Technologies and Applications (ADTTA'99), Praha (Pruhonice), 7–11 June 1999, Czech Republic*, Paper # P-C24 on the ADTTA'99 Web page and Proceedings CD; Numerical values of measured cross sections are tabulated in Yu. E. Titarenko, *Experimental and Theoretical Study of the Yields of Residual Product Nuclei Produced in Thin Targets Irradiated by 100–2600 MeV Protons*," Final Project Technical Report of ISTC 839B-99, ITEP, Moscow (2001).

65. Arthur C. Wahl, "Systematics of Fission-Product Yields," Los Alamos National Laboratory Report LA-UR-01-5944, Los Alamos (2001).

66. A. Ferrari, "Physics and Modeling of Hadronic Interactions," Tutorials, Int. Conf. on Advanced Monte Carlo for Radiation Physics, Particle Transport Simulation and Application (MC 2000), 23–26 October, 2000, Lisbon, Portugal; more references and many details on FLUKA may be found at the Web page http://pcfluka.mi.infn.it/.

67. M. Veselsky, "Production Mechanism of Hot Nuclei in Violent Collisions in the Fermi Energy Domain," E-print: nucl-th/0107062 v2 (8 October 2001);

M. Veselsky *et al.* "Production of Fast Evaporation Residues by the Reaction ^{20}Ne + ^{208}Pb at Projectile Energies of 8.6, 11.4 and 14.9 A.MeV," *Z. Phys.* **A356**, 4003–410 (1997).

68. S. G. Mashnik, A. J. Sierk, O. Bersillon, and T. Gabriel, "Cascade-Exciton Model Analysis of Proton Reactions from 10 MeV to 5 GeV", Los Alamos National Laboratory Report LA-UR-97-2905 (1997); http://t2.lanl.lanl.gov/publications/publications.html.

69. H. H. K. Tang, G. R. Srinivasan, and N. Azziz, "Cascade Statistical Model for Nucleon-Induced Reactions on Light Nuclei in the Energy Range 50 MeV–1 GeV", *Phys. Rev. C* **42**, 1598–1622 (1990).

70. V. S. Barashenkov and A. Polanski, "Electronic Guide for Nuclear Cross-Sections", Joint Institute for Nuclear Research Report JINR E2-94-417, Dubna, Russia (1994).

71. A. Auce *et al.*, "Reaction Cross Section for 75–190 MeV Alpha Particles on Targets from ^{12}C to ^{208}Pb," *Phys. Rev. C* **50**, 871–879 (1994).

72. L. V. Dubar, D. Sh. Eleukenov, L. I. Slyusarenko, and N. P. Yurkuts, "Parameterization of the Total Cross Sections of Reactions in the Intermediate Energy Region," *Yad. Fiz.* **49**, 1239–1242 (1989) [*Sov. J. Nucl. Phys.* **49**, 771–773 (1989)].

73. A. Chatterjee, K. H. N. Murthy, and S. K. Gupta, "Optical Reaction Cross-Section for Light Projectiles," *Pramana* **16**, 391–402 (1981).

74. G. S. Mani, M. A. Melkanoff, and A. Zucker, Centre d'Etudes Nucleaire de Saclay Report CEA 2380 (1963).

75. K. K. Gudima, G. Röpke, H. Schulz, and V. D. Toneev, "The Coalescence Model and Pauli Quenching in High-Energy Heavy-Ion Collisions," Joint Institute for Nuclear Research Report JINR-E2-83-101, Dubna (1983); H. Schulz, G. Röpke, K. K. Gudima, and V. D. Toneev, "The Coalescence phenomenon and the Pauli Quenching in High-Energy Heavy- Ion Collisions," *Phys. Lett.* **B124** 458–460 (1983); V. D. Toneev and K. K. Gudima, "Particle Emission in Light and Heavy-Ion Reactions," *Nucl. Phys.* **A400** 173c–190c (1983).

76. Joseph I. Kapusta, "Mechanisms for Deuteron Production in Relativistic Nuclear Collisions," *Phys. Rev. C* **21**, 1301–1310 (1980).

77. N. V. Stepanov, "Statistical Simulation of Excited Nuclei Fission. 1. Formulation of the Model", ITEP Preprint 81 (1987), Institute for Theoretical and Experimental Physics, Moscow, USSR (1987); N. V. Stepanov, "Statistical Simulation of Excited Nuclei Fission. 2. Calculations and Comparison with Experiment," ITEP Preprint 55-88 (1988), Institute for Theoretical and Experimental Physics, Moscow, USSR (1988).

78. J. R. Wu and C. C. Chang, "Complex-Particle Emission in the Pre-Equilibrium Exciton Model," *Phys. Rev. C* **17**, 1540–1549 (1978).

79. Konstantin K. Gudima, Stepan G. Mashnik, and Arnold J. Sierk, "User Manual for the Code LAQGSM," Los Alamos National Laboratory Report LA-UR-01-6804, Los Alamos (2001); http://lib-www.lanl.gov/la-pubs/00818645.pdf.

80. S. G. Mashnik *et al.*, " Benchmarking Codes for Proton Radiography Applications," *Proc. 6th Intl. Workshop on Shielding Aspects of Accelerators, Targets and Irradiation Facilities (SATIF-6), April 10–12, 2002, Stanford Linear Accelerator Center, CA 94025, USA*; http://www.nea.fr/html/science/satif/3-03.html LANL Report LA-UR-02-0609, Los Alamos (2002).

81. Ray E. L. Green and Ralph G. Korteling, "Implications for Statistical Theories of Fragmentation from Measurements of $Ag(p,^3He)$ and $Ag(p,^4He)$ at Intermediate Proton Energies," *Phys. Rev. C* **18**, 311–316 (1978); tabulated values are available from the EXFOR database at the Web page: http://www.nea.fr/html/dbdata/x4/.

82 Ray E. L. Green, Ralph G. Korteling, and K. Peter Jackson, "Inclusive Production of Isotopically Resolved Li through Mg Fragments by 480 MeV p + Ag Reactions," *Phys. Rev. C* **29**, 1806–1824 (1984).

83 R. J. Charity *et al.*, "Systematics of Complex Fragment Emission in Niobium-induced Reactions", *Nucl. Phys.* **A483**, 371–405 (1988); R. J. Charity, "$N - Z$ Distributions of Secondary Fragments and the Evaporation Attractor Line", *Phys. Rev. C* **58**, 1073–1077 (1998); R. J. Charity *et al.*, "Emission of Unstable Clusters from Yb Compound Nuclei," *Phys. Rev. C* **63**, 024611 (2001); http://wunmr.wustl.edu~rc/.